iScience

CellPress

Article

A CRISPR Screen Identifies LAPTM4A and TM9SF Proteins as Glycolipid-Regulating Factors

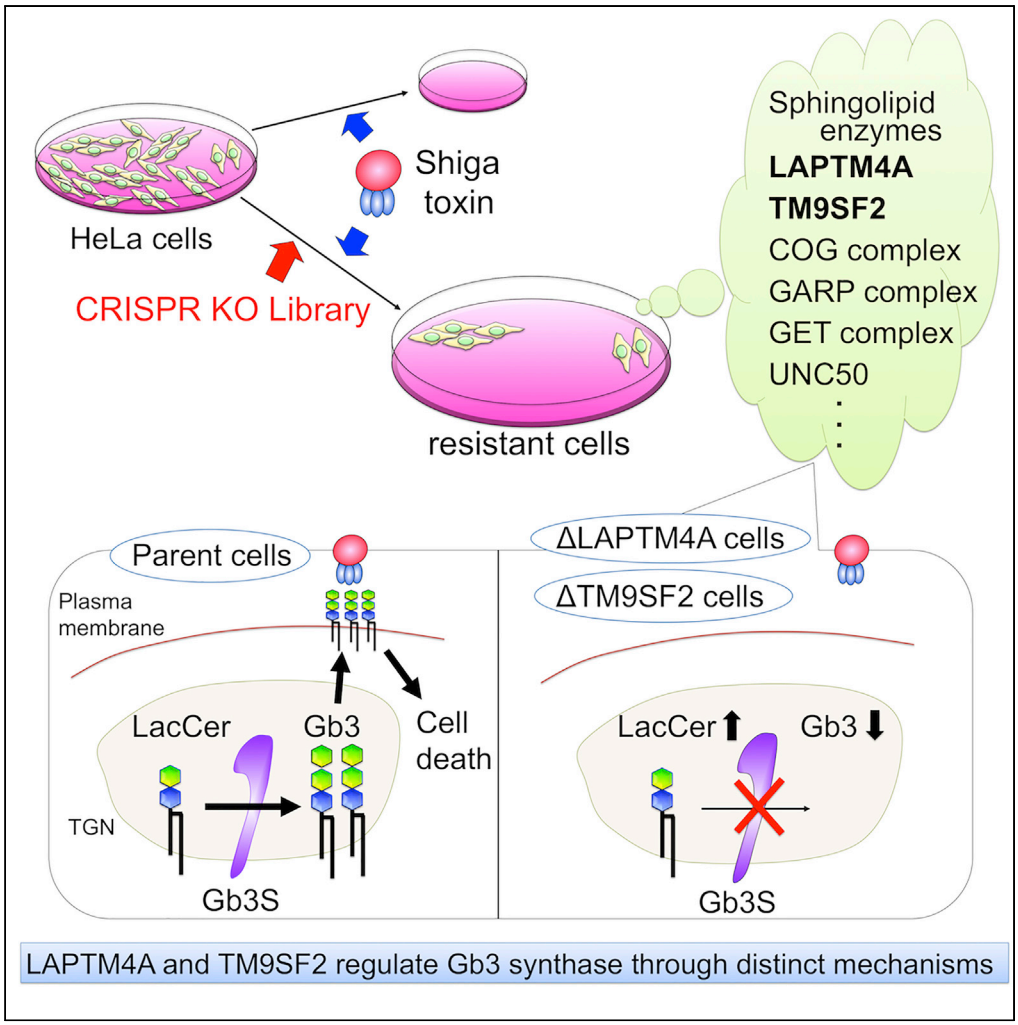

Toshiyuki Yamaji, Tsuyoshi Sekizuka, Yuriko Tachida, Chisato Sakuma, Kanta Morimoto, Makoto Kuroda, Kentaro Hanada

tyamaji@nih.go.jp

HIGHLIGHTS

Genome-wide CRISPR knockout screening using Shiga toxin-induced cell death

Both LAPTM4A and TM9SF2 are required for Gb3 biosynthesis

Loss of LAPTM4A reduces Gb3 synthase activity post-transcriptionally

TM9SF2 regulates the subcellular localization of Gb3 synthase

DATA AND SOFTWARE AVAILABILITY

GSE116730

Yamaji et al., iScience *11*, 409–424
January 25, 2019
https://doi.org/10.1016/j.isci.2018.12.039

iScience

CellPress

Article

A CRISPR Screen Identifies LAPTM4A and TM9SF Proteins as Glycolipid-Regulating Factors

Toshiyuki Yamaji,[1,5,*] Tsuyoshi Sekizuka,[2] Yuriko Tachida,[1,4] Chisato Sakuma,[1] Kanta Morimoto,[1,3] Makoto Kuroda,[2] and Kentaro Hanada[1]

SUMMARY

Glycosphingolipids (GSLs) are produced by various GSL-synthesizing enzymes, but post-translational regulation of these enzymes is incompletely understood. To address this knowledge disparity, we focused on biosynthesis of globotriaosylceramide (Gb3), the Shiga toxin (STx) receptor, and performed a genome-wide CRISPR/CAS9 knockout screen in HeLa cells using STx1-mediated cytotoxicity. We identified various genes including sphingolipid-related genes and membrane-trafficking genes. In addition, we found two proteins, LAPTM4A and TM9SF2, for which physiological roles remain elusive. Disruption of either *LAPTM4A* or *TM9SF2* genes reduced Gb3 biosynthesis, resulting in accumulation of its precursor, lactosylceramide. Loss of LAPTM4A decreased endogenous Gb3 synthase activity in a post-transcriptional mechanism, whereas loss of TM9SF2 did not affect Gb3 synthase activity but instead disrupted localization of Gb3 synthase. Furthermore, the Gb3-regulating activity of TM9SF2 was conserved in the TM9SF family. These results provide mechanistic insight into the post-translational regulation of the activity and localization of Gb3 synthase.

INTRODUCTION

Glycosphingolipids (GSLs) are ubiquitously expressed in animals and are essential for embryonic development (Yamashita et al., 1999). Mammalian cells produce a variety of GSLs, depending on the cell and tissue types. Various physiological roles of GSLs have been identified, including cell adhesion and cell signaling (Hakomori, 2008). In addition, several GSLs are exploited as membrane receptors by toxins and infectious agents. For example, globotriaosylceramide (Gb3) serves as the receptor of Shiga toxin (STx) produced by enterohemorrhagic *Escherichia coli* and *Shigella dysenteriae*, whereas the ganglioside GM1 serves as the receptor of cholera toxin produced by *Vibrio cholerae* (Hanada, 2005). Gb3 also has other biological significance, especially under pathological conditions, including tumor metastasis (Kovbasnjuk et al., 2005) and Fabry diseases, caused by α-galactosidase A deficiency (Clarke, 2007). Loss of Gb3 and the corresponding globo-series GSLs in mice results in higher sensitivity to lipopolysaccharides (Kondo et al., 2013), indicating that the balance of GSLs affects inflammation. Therefore, the regulatory mechanisms of GSL synthesis and degradation are important for understanding various physiological and pathological states.

The overall structure of complex glycan moieties in GSLs is highly diverse. Nevertheless, their core portion is conserved; the hydrophobic moiety of GSLs is commonly composed of ceramides, which are synthesized in the ER. After transport from the ER to the late Golgi complex by the ceramide transport protein CERT (Hanada et al., 2003), ceramide is converted to sphingomyelin, a major phosphosphingolipid in mammals. On the other hand, if ceramide is transported to the early Golgi region through a CERT-independent mechanism, ceramide is converted to glucosylceramide (GlcCer), which is the common precursor of all GSLs, with exception to galactosylceramide and its derivatives (Ichikawa et al., 1996). After traversing across the Golgi membrane, GlcCer is converted to lactosylceramide (LacCer) in the luminal side of the Golgi complex (Kumagai et al., 2010). LacCer is converted to one of several types of trihexosyl ceramides, which in mammals are composed predominately of Gb3 and GM3. Gb3 is synthesized from LacCer by α1,4 galactosyltransferase (hereafter referred to as Gb3 synthase; encoded by the *A4GALT* gene in the human genome), which is mainly localized to the *trans*-Golgi network (TGN) (Kojima et al., 2000; Yamaji and Hanada, 2015; D'Angelo et al., 2013).

Proper glycosylation of GSLs requires not only transcriptional regulation of GSL enzyme genes but also post-translational regulation of these enzymes, including the regulation of enzymatic activities, subcellular

[1]Department of Biochemistry and Cell Biology, National Institute of Infectious Diseases, 1-23-1 Toyama, Shinjuku-ku, Tokyo 162-8640, Japan

[2]Pathogen Genomics Center, National Institute of Infectious Diseases, 1-23-1 Toyama, Shinjuku-ku, Tokyo 162-8640, Japan

[3]Department of Materials and Applied Chemistry, College of Science and Technology, Nihon University, Chiyoda-ku, Tokyo 101-8308, Japan

[4]Present address: Glycometabolic Biochemistry Laboratory, RIKEN, Wako, Saitama 351-0198, Japan

[5]Lead Contact

*Correspondence: tyamaji@nih.go.jp

https://doi.org/10.1016/j.isci.2018.12.039

distributions, and transports. For example, the conserved oligomeric Golgi (COG) complex maintains Golgi-resident glycan enzymes by retrograde trafficking (Blackburn and Lupashin, 2016), and defects in COG subunits are linked to Congenital Disorders of Glycosylation-type II, a group of inherited metabolic disorders (Zeevaert et al., 2008). However, the mechanisms of post-transcriptional glycosyltransferase regulation in the Golgi and TGN are incompletely understood.

To further elucidate mechanisms of post-transcriptional GSL regulation, we focused on the biosynthesis of the STx receptor Gb3 and performed a genome-wide CRISPR/CAS9 knockout (KO) screen (Shalem et al., 2014; Wang et al., 2014) in HeLa cells using STx1-induced cytotoxicity as our screening criteria. This allowed for unbiased identification of intracellular factors affecting the activity and localization of the Gb3-related enzymes through screening for gene mutations conferring STx resistance. This approach identified two multispanning membrane proteins, lysosomal protein transmembrane 4α (LAPTM4A) and transmembrane 9 superfamily 2 (TM9SF2). Loss of either protein resulted in reduction of Gb3 levels and subsequent STx resistance. Biochemical and cell biological analyses revealed that LAPTM4A and TM9SF2 regulated Gb3 synthase through distinct mechanisms, providing insight into previously unrecognized mechanisms for post-translational regulation of GSL synthases.

RESULTS

Identification of Genes Conferring Resistance to STx-Induced Cell Death

To identify host factors involved in the regulation of Gb3 biosynthesis by exploiting STx sensitivity as an indicator of cellular Gb3 levels, we performed a genome-wide CRISPR/CAS9 KO screen in HeLa cells. We used a lentivirus-based GeCKO v2 pooled library, which is delivered as two half-libraries (A and B) targeting a total of 19,050 human genes with six single guide RNAs (sgRNAs) per gene (Sanjana et al., 2014). Two independent sgRNA-expressing cell libraries (A-1, A-2, B-1, B-2) were prepared by transducing the lentivirus libraries, and cells were then treated with STx1 to assess toxicity. The sgRNAs integrated into the cellular genomes of surviving cells were amplified by PCR and analyzed with high-throughput sequencing. sgRNAs enriched by STx in both independent cell libraries were selected as STx-resistance sgRNA candidates (Figure 1A, the full raw dataset is shown in Data S1 and S2). The candidates included 167 sgRNAs for 97 genes, with 31 genes containing multiple sgRNAs. The enriched gene candidates included nearly all sphingolipid-related genes, including *A4GALT* (Gb3 synthase) and *B4GALT5* (LacCer synthase), and various membrane trafficking genes, including the COG complex (*COG1-8*) involved in intra-Golgi retrograde transport (Blackburn and Lupashin, 2016), the GARP complex (*VPS51-54*) involved in late endosome–TGN retrograde transport (Bonifacino and Hierro, 2011), the GET complex (*GET4, CAMLG*) involved in ER translocation of tail-anchored membrane proteins (Stefanovic and Hegde, 2007), and *UNC50,* which is involved in late endosome-TGN STx retrograde transport, as was recently identified (Selyunin et al., 2017).

For validation of this screen, 21 identified sgRNAs were individually transduced into HeLa cells to identify the effect of these sgRNAs on STx-induced cytotoxicity (Figure 1B). Most sgRNAs conferred resistance to STx. Furthermore, the degrees of resistance and the fold enrichment of each sgRNA (shown in Figure 1A) were highly correlated, indicating the reproducibility of this screening approach. Figure 1C shows the Gb3 biosynthesis pathway. The sgRNAs of all sphingolipid-related enzymes and transporters shown in this pathway were enriched in the screen (Figure 1D). Among these genes, we established KO cell clones of three genes, including serine palmitoyltransferase small subunit A (*SPTSSA*) (Han et al., 2009), acetyl-CoA carboxylase alpha (*ACACA*), and transmembrane protein 165 (*TMEM165*), a Mn^{2+} transporter required for some glycosyltransferases (Potelle et al., 2016), using the CRISPR/CAS system. We confirmed that disruption of these genes reduced or completely inhibited Gb3 biosynthesis and reduced STx binding, which was reversed by the addition of sphingosine to *SPTSSA*-KO cells, addition of palmitate to *ACACA*-KO cells, and TMEM165 cDNA transfection in *TMEM165*-KO cells (Figure S1).

Inhibition of Gb3 Synthesis in LacCer in *LAPTM4A*- and *TM9SF2*-KO Cells

Among the enriched gene candidates shown in Figure 1A, we focused on two multispanning membrane protein genes, *LAPTM4A* and *TM9SF2*, as multiple sgRNAs for these genes were highly enriched in the screen, but their role in STx-induced cell death were as yet unknown. To confirm resistance to STx, KO cell clones of each gene were generated using the CRISPR/CAS system. Sequence analyses demonstrated that coding regions within exon 1 of the respective genes in the *LAPTM4A*- and *TM9SF2*-KO cell clones (ΔLAPTM4A and ΔTM9SF2) were frame-shifted in all alleles (Figure 2A). Furthermore, expression of these

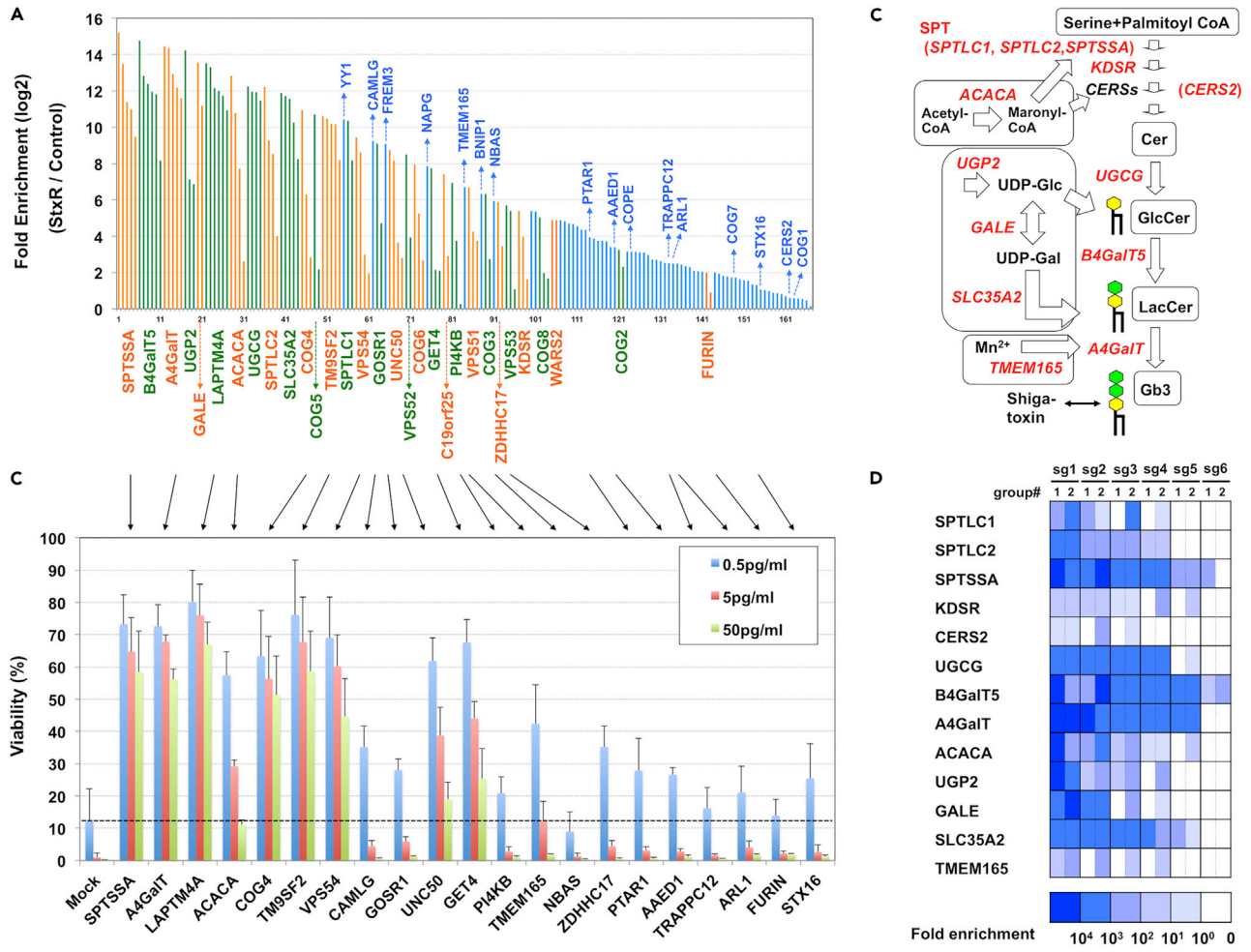

Figure 1. Identification of STx Resistance Genes in a Genome-Wide CRISPR Screen

(A) Identification sgRNAs enriched in the screen. Fold enrichment represents the average of two independent experiments. Orange and green bars indicate that multiple sgRNAs were enriched in a gene, whereas blue bars indicate that a single sgRNA was enriched in a gene. The full raw dataset is shown in Data S2.

(B) Reproducibility of STx resistance conferred by individual sgRNAs. Each sgRNA was transduced into HeLa cells. Untransfected cells were excluded using puromycin selection, and successfully transfected cells were then treated with STx1 at the indicated concentration. Viability was estimated using an MTT assay and is expressed as the percentage of the MTT value (OD570) in the absence of STx1. Percentage shown is mean percentage ±SD obtained from three independent experiments. Arrows indicate that the sgRNAs shown in Figure 1A correspond to the sgRNAs in this figure. The dotted line indicates the viability of mock-transfected cells treated with 0.5 pg/mL STx1.

(C) Gb3 biosynthetic pathway. Genes enriched in the screen are shown in red.

(D) Fold enrichment of six sgRNAs in sphingolipid-related genes shown in Figure 1C. Heatmap is representative individual sgRNA enrichment (sg1-6) in two independent experiments (group #1 and 2).

See also Figure S1 and Data S1, S2, and S3.

proteins was lost in KO cells, as revealed by western blot analysis (Figure 2B). The KO cells were highly resistant to STx-induced cell death (Figure 2C), and cell surface STx binding was also lost (Figure 2D). Introduction of wild-type *LAPTM4A* and *TM9SF2* cDNA into the respective KO cell lines (ΔLAPTM4A/LAPTM4A and ΔTM9SF2/TM9SF2) resulted in full recovery of cell surface Gb3 levels and STx sensitivity (Figures 2C and 2D), verifying that disruptions of *LAPTM4A* and *TM9SF2* were the causative mutations for Gb3-related phenotypes in mutant cells.

To determine if Gb3 biosynthesis was affected by the disruption of *LAPTM4A* and *TM9SF2*, we metabolically labeled lipids with [^{14}C]galactose and analyzed the labeled lipids using thin-layer chromatography (TLC) and radioactive imaging (Figures 2E and 2F). Relative to parent cells, *LAPTM4A*- and *TM9SF2*-KO

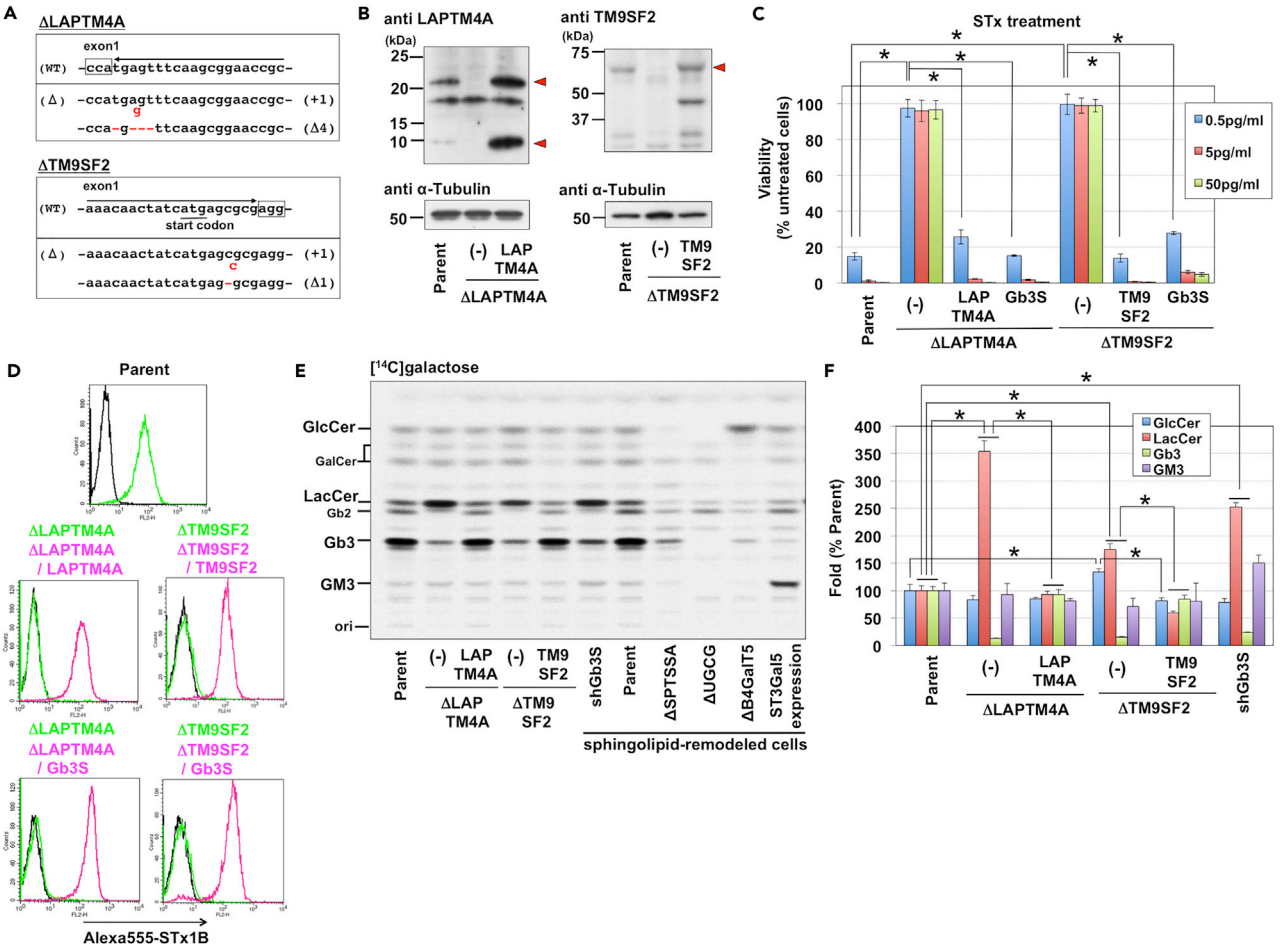

Figure 2. Requirement of LAPTM4A and TM9SF2 for Gb3 Biosynthesis

(A) Construction of *LAPTM4A*- and *TM9SF2*-KO HeLa cells. Red letters in sequences are indicative of deletion or insertion mutations, which cause frameshifts shown at the right side of the sequences. Boxes indicate protospacer adjacent motif (PAM) sequences.

(B) Western blot analysis of KO cells and cDNA-rescued cells. Parent cells (HeLa mCAT#8), *LAPTM4A*- and *TM9SF2*-KO cells (ΔLAPTM4A and ΔTM9SF2; "-" is indicative of cDNA-unintroduced cells), and corresponding cDNA-reintroduced cells (ΔLAPTM4A/LAPTM4A and ΔTM9SF2/TM9SF2) were analyzed. Triangles are indicative of target proteins.

(C) STx sensitivity in KO cells and cDNA-reintroduced cells. Cells shown in B and Gb3S-introduced KO cells were treated with STx1 at the indicated concentrations. Viability was estimated as described in Figure 1B and is expressed as the mean percentage ±SD obtained from three independent experiments. The Bonferroni corrected t test was used for multiple comparisons. *, $p < 0.0083$.

(D) Surface binding of STx on KO cells and corresponding cDNA-rescued cells. Cells shown in C were stained with (yellow-green and magenta lines) or without (black line) Alexa555-labeled STx1 B subunit (Alexa 555-STx1B) and analyzed using FACS. Black and magenta lines indicate staining in KO cells expressing the indicated cDNAs, and yellow-green lines indicate staining in KO cells without introduction of cDNA.

(E) GSL metabolic analysis of KO cells and corresponding cDNA-rescued cells. Cells shown in B were labeled with [^{14}C]galactose, and labeled lipids treated by mild alkali-catalyzed methanolysis were separated on a TLC plate. To assess lipids accurately, labeled lipids in sphingolipid-remodeled HeLa cells were used as markers, shown at the right side of the samples. UGCG is GlcCer synthase. B4GalT5 is a major LacCer synthase. ST3Gal5 is GM3 synthase.

(F) Quantification of labeling experiments shown in E. The relative amount of each [^{14}C]galactose-labeled lipid is expressed as the percentage of band intensity in parent cells and is representative of the mean percentage ±SD obtained from three independent experiments. The Bonferroni corrected t test was used for multiple comparisons. *, $p < 0.01$.

cells produced lower levels of labeled Gb3 (12.9 ± 0.9% in *LAPTM4A*-KO cells and 15.4 ± 0.5% in *TM9SF2*-KO cells) and had higher levels of labeled LacCer, the direct precursor of Gb3 (353.9 ± 19.5% in *LAPTM4A*-KO cells and 175.3 ± 10.4% in *TM9SF2*-KO cells). These labeling patterns in the two mutant cell lines were similar to that of Gb3 synthase knockdown cells (shGb3S). Notably, introduction of wild-type *Gb3 synthase* cDNA into *LAPTM4A*- and *TM9SF2*-KO cells restored both labeled Gb3 levels and STx sensitivity (Figures 2C and 2D). Taken together, these results suggested that LAPTM4A and TM9SF2 were involved in Gb3 synthase-dependent conversion of LacCer to Gb3.

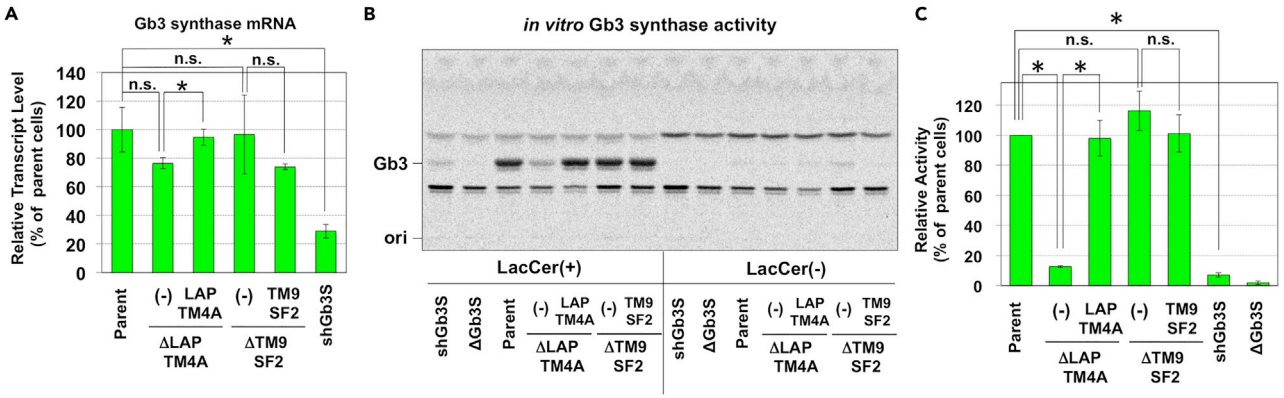

Figure 3. Loss of LAPTM4A, but Not TM9SF2, Reduces Gb3 Synthase Activity Post-transcriptionally

(A) Quantitative real-time PCR of Gb3 synthase mRNA. Relative mRNA levels of Gb3 synthase are expressed as the percentage of the value in parent cells and are representative of the mean percentage ±SD obtained from three independent experiments. The Bonferroni corrected t test was used for multiple comparisons. *, $p < 0.01$.

(B) Measurement of Gb3 synthase activity *in vitro*. Cell lysates were incubated with (left side) or without (right side) LacCer in addition to [^{3}H]UDP-galactose, and labeled lipids were separated on a high-performance TLC plate.

(C) Quantification of labeling experiments shown in B. Relative Gb3 synthase activities are expressed as percentage of the value in control cells and are representative of mean percentage ±SD obtained from three independent experiments. The Bonferroni corrected t test was used for multiple comparisons. *, $p < 0.01$.

See also Figure S2.

Loss of LAPTM4A, but Not TM9SF2, Reduced Gb3 Synthase Activity Post-transcriptionally

Next, the transcriptional level of *Gb3 synthase* was examined in KO cells (Figure 3A). *Gb3 synthase* transcript levels were unchanged in *TM9SF2*-KO cells (lane 4 vs. lanes 1 and 5). *Gb3 synthase* mRNA was modestly decreased in *LAPTM4A*-KO cells (lane 2 vs. lane 3), but this change was not statistically significant compared with control cells (lane 2 vs. lane 1). As a reference, Gb3 synthase-knockdown (shGb3S) cells, which had similar Gb3 levels to *LAPTM4A*-KO cells (Figures 2E and 2F), had a significant reduction of *Gb3 synthase* mRNA (28.9 ± 4.6% compared with the parent cells) (lane 6 vs. lane 1). Taken together, these data suggested that decreased Gb3 levels in *LAPTM4A*- and *TM9SF2*-KO cells were unlikely to be due to transcriptional down-regulation of the *Gb3 synthase* gene. The contribution of post-translational mechanisms, including changes to the stability of Gb3 synthase proteins, was then examined. To this aim, we first attempted to detect endogenous Gb3 synthase proteins using antibodies against Gb3 synthase but were unsuccessful, likely due to low protein abundance (Figure S2). Therefore, we next attempted to measure the enzymatic activity of endogenous Gb3 synthase *in vitro* (Figures 3B and 3C). Intriguingly, Gb3 synthase activity was markedly decreased in *LAPTM4A*-KO cell lysates relative to wild-type. This reduction was recovered to wild-type levels by the introduction of wild-type *LAPTM4A* cDNA. Contrastingly, *TM9SF2* disruption did not affect *in vitro* activity of Gb3 synthase. Taken together, these results indicated that LAPTM4A was involved in the regulation of Gb3 synthase activity or protein abundance, whereas TM9SF2 regulation of Gb3 synthesis was independent of these mechanisms. It should be noted that abundance of exogenously expressed Gb3 synthase was not changed in *LAPTM4A*-KO cells relative to parent cells (Figure S2G).

Molecular Assessment of LAPTM4A Regulation of Gb3 Synthesis

LAPTM4A has four predicted transmembrane domains followed by a C-terminus cytoplasmic tail that contains PY (Leu/Pro-Pro-X-Tyr) motifs for binding of the ubiquitin ligase NEDD4, which is required for lysosomal localization (Figure 4A) (Milkereit and Rotin, 2011). We therefore investigated whether the lysosomal localization of LAPTM4A is required for regulation of Gb3 biosynthesis using a deletion mutant lacking the C-terminal region (LAPTM4AΔC-HA) (Figures 4A and 4B). HA-tagging of LAPTM4A at either the N or C terminus (HA-LAPTM4A or LAPTM4A-HA) had no effect on LAPTM4A regulation of Gb3, and both tagged wild-type proteins recovered STx binding when expressed in *LAPTM4A*-KO cells (Figures 4C and 4D). Intriguingly, deletion of the C-terminal region (LAPTM4AΔC-HA) still maintained Gb3-regulating activity, and the mutant restored defective STx binding in *LAPTM4A*-KO cells (Figures 4C and 4D). Immunostaining analysis with anti-HA revealed that LAPTM4AΔC-HA proteins were mainly localized to the ER (VAP-A), whereas wild-type LAPTM4A-HA and HA-LAPTM4A were mainly localized to lysosomes (LAMP2) and

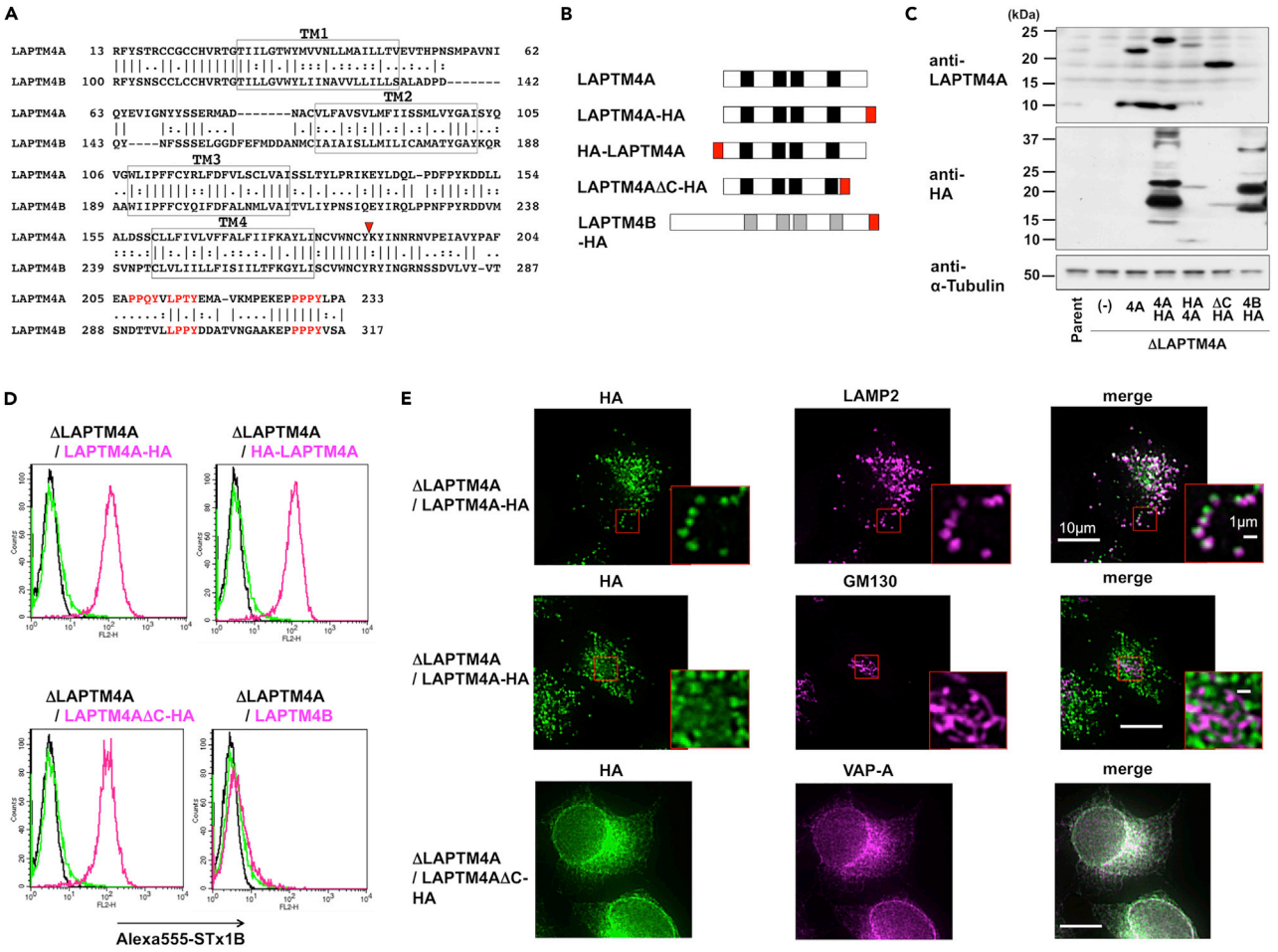

Figure 4. LAPTM4B Does Not Compensate for Loss of LAPTM4A, and the NEDD4-Binding Region of LAPTM4A Is Dispensable for Regulation of Gb3 Biosynthesis

(A) Alignment of LAPTM4A and its paralog LAPTM4B. Boxes are indicative of transmembrane domains. Red letters indicate PY motifs (L/PPxY), which can bind to the E3 ubiquitin ligase NEDD4. The triangle is indicative of the C-terminal truncation site (LAPTM4AΔC).

(B) Schematics of LAPTM4A, HA-tagged and mutant proteins, and LAPTM4B used in this study. Red boxes indicate HA-tags, and black and gray boxes indicate transmembrane domains.

(C) Western blot analysis of stable transfectants expressing the proteins shown in B. Lysates from parent cells, LAPTM4A KO cells (ΔLAPTM4A), and ΔLAPTM4A cells expressing the indicated proteins were used in analysis. Note that the expression level of LAPTM4AΔC-HA was apparently low when anti-HA was used. However, LAPTM4AΔC-HA was detected by anti-LAPTM4A more clearly than anti-HA compared with wild-type LAPTM4A-HA, indicating that LAPTM4AΔC-HA was sufficiently expressed.

(D) Surface binding of STx on transfected cells. The indicated cells were stained with (yellow-green and magenta lines) or without (black line) Alexa555-STx1B and analyzed by FACS. Black and magenta lines indicate staining in KO cells expressing the indicated cDNAs, and yellow-green lines indicate staining in KO cells without introduction of cDNA.

(E) Intracellular localization of LAPTM4A-HA and LAPTM4AΔC-HA. ΔLAPTM4A/LAPTM4A-HA and ΔLAPTM4A/LAPTM4AΔC-HA cells were stained with anti-HA antibodies and the indicated marker antibodies (anti-LAMP2 [lysosome and late endosome], anti-GM130 [Golgi], anti-VAP-A [ER]). Scale bars, 10 μm and 1 μm.

See also Figure S3.

late endosomes (Rab9) (Figures 4E, S3A, and S3B). Taken together, these results suggested that lysosomal and late endosomal localization of LAPTM4A was unlikely to be required for regulation of Gb3 biosynthesis. When these images were carefully observed, we found that LAPTM4A-HA, HA-LAPTM4A, and LAPTM4AΔC-HA were all partially localized to the Golgi apparatus (GM130), suggesting that these proteins may also function in the Golgi (Figures 4E, S3C, and S3D).

Next, to assess intracellular localization of Gb3 synthase, moxNeonGreen fluorescent protein (Costantini et al., 2015; Shaner et al., 2013) was fused to the C-terminus of Gb3 synthase (Gb3S-NG),

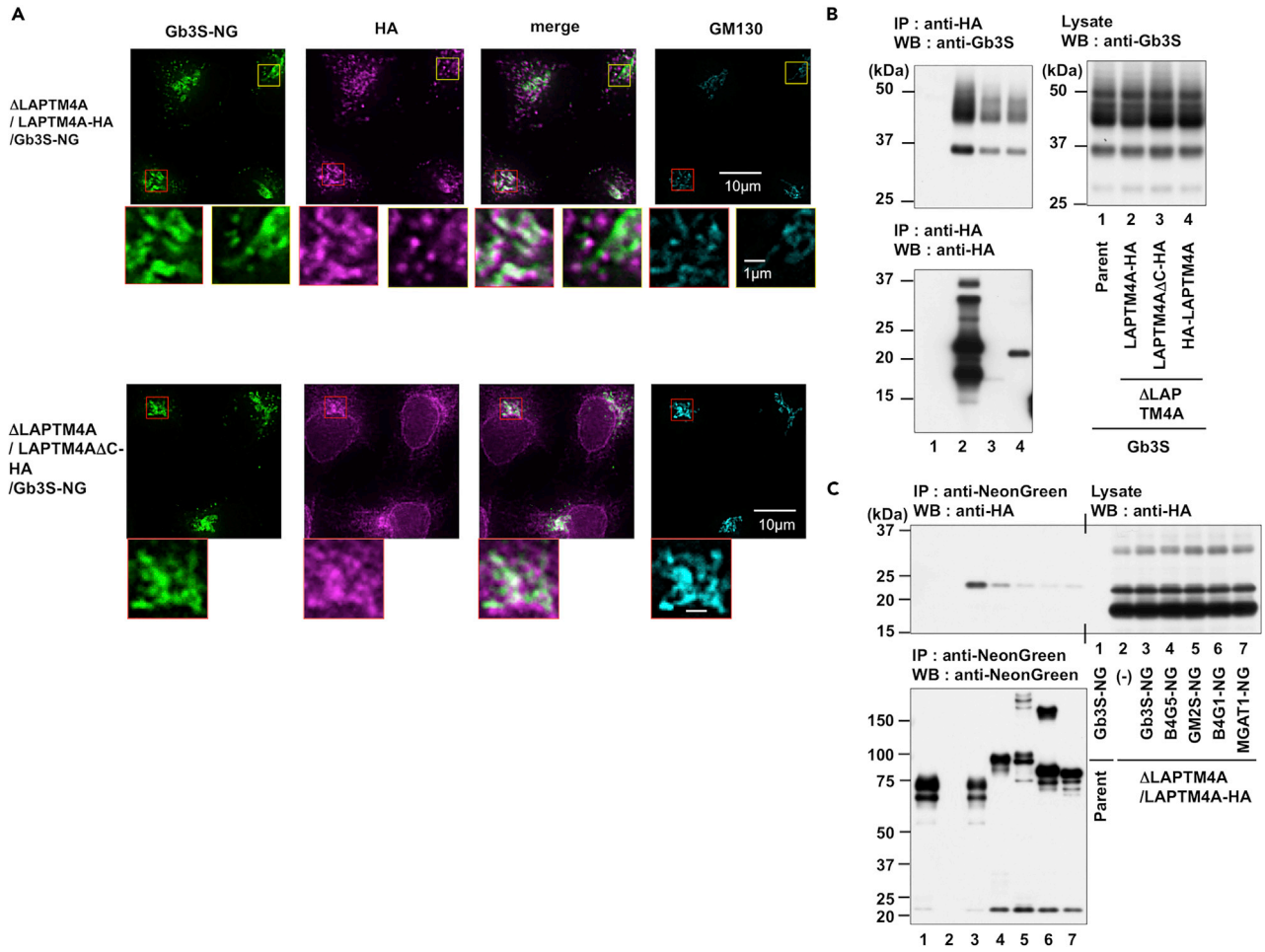

Figure 5. LAPTM4A Interacts with Gb3 Synthase

(A) Intracellular localization of LAPTM4A-HA and LAPTM4AΔC-HA in Gb3S-NG-expressing cells. ΔLAPTM4A/LAPTM4A-HA/Gb3S-NG and ΔLAPTM4A/LAPTM4AΔC-HA/Gb3S-NG cells were stained with anti-HA and anti-GM130 antibodies. Scale bars, 10 μm and 1 μm.

(B) Co-immunoprecipitation of Gb3 synthase with LAPTM4A. Parent-Gb3S, ΔLAPTM4A/LAPTM4A-HA/Gb3S, ΔLAPTM4A/LAPTM4AΔC-HA/Gb3S, and ΔLAPTM4A/HA-LAPTM4A/Gb3S cells were lysed and immunoprecipitated with anti-HA agarose. Immunoprecipitates (IP) and lysates were subjected to SDS-PAGE and western blot (WB) analyses with the indicated antibodies.

(C) Co-immunoprecipitation of LAPTM4A with glycosyltransferases. Parent/Gb3S-NG cells and ΔLAPTM4A/LAPTM4A-HA cells expressing Gb3S-NG, B4GalT5 (B4G5)-NG, GM2 synthase (GM2S)-NG, B4GalT1 (B4G1)-NG, and MGAT1-NG were lysed and immunoprecipitated with anti-NeonGreen magnet beads. Immunoprecipitates (IP) and lysates were subjected to SDS-PAGE and western blot (WB) with the indicated antibodies.

See also Figure S4.

and fusion proteins were retrovirally expressed in parent cells (Parent/Gb3S-NG), *LAPTM4A*-KO cells (ΔLAPTM4A/Gb3S-NG), and LAPTM4A-rescued cells (ΔLAPTM4A/LAPTM4A-HA/Gb3S-NG and ΔLAPTM4A/LAPTM4AΔC-HA/Gb3S-NG). Gb3S-NG was mainly localized to the Golgi (likely including the TGN) in both parent and *LAPTM4A*-KO cells, although some dispersed punctate structures were observed in a few cell populations. The similar localization patterns of Gb3S-NG suggested that LAPTM4A did not affect localization of Gb3 synthase (Figure S4). In Gb3S-NG-expressing cells, LAPTM4A-HA and LAPTM4AΔC-HA were partially co-localized with Gb3S-NG at the Golgi apparatus (Figure 5A). In particular, in addition to a weak staining of LAPTM4A-HA at the Golgi seen in some cell populations (indicated by the yellow box in Figure 5A) such as Gb3S-NG-unexpressing cells (Figure 4E), strong staining of LAPTM4A-HA at the Golgi was observed in some cell populations, and the staining co-localized with Gb3-NG (red box in Figure 5A). These results prompted us to investigate the interaction between LAPTM4A and Gb3 synthase. Therefore, we performed immunoprecipitation analysis using LAPTM4A and Gb3S-coexpressing cells. When anti-HA-agarose was used, Gb3 synthase co-immunoprecipitated with LAPTM4A-HA,

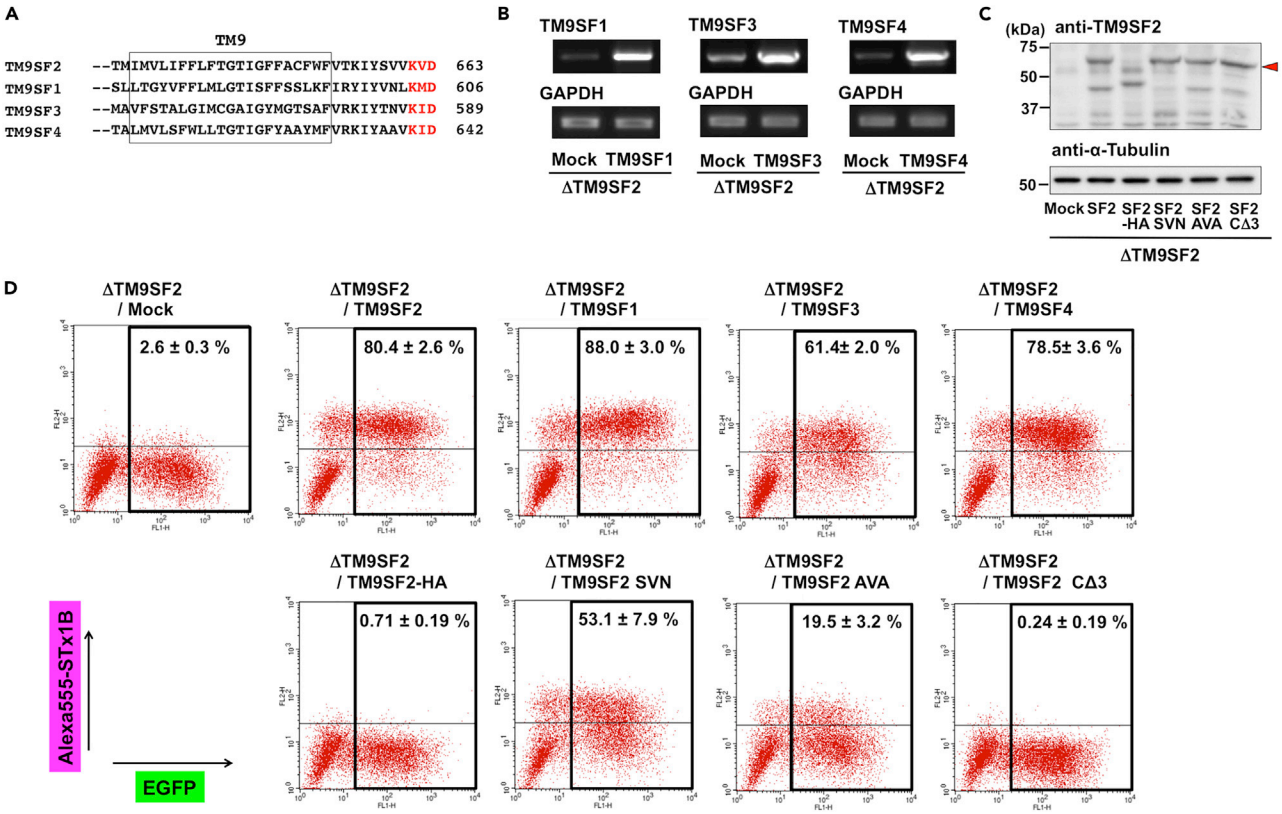

Figure 6. Gb3 Regulation Is Conserved in TM9SF Family Proteins, and the C-terminus of TM9SF2 is Functionally Essential

(A) Alignment of C-terminal regions in TM9SF family proteins. Boxes are indicative of transmembrane domains. Red letters are indicative of predicted COPI-binding sites.

(B) RT-PCR analysis of *TM9SF1*, *3*, and *4* mRNAs from transient transfectants expressing these TM9SFs.

(C) Western blot analysis of transient transfectants expressing HA-tagged TM9SF2 and TM9SF2 mutant proteins. Triangles indicate target proteins.

(D) Effects of TM9SF2 family proteins and TM9SF2 mutant proteins on STx binding. cDNAs coding the specified proteins were transiently transfected with EGFP cDNA into *TM9SF2*-KO cells, and cells were stained with Alexa555-STx1B and analyzed by FACS. EGFP-positive cells were gated, and the percentage of STx-binding positive cells is expressed and is representative of the mean percentage ±SD obtained from three independent experiments.

See also Figures S5 and S6.

HA-LAPTM4A, and LAPTM4AΔC-HA (Figure 5B). No band was detected when only Gb3S was expressed, suggesting that these interactions were specific. Next, several glycosyltransferase-NG fusion proteins (B4GalT5 (B4G5), GM2 synthase (GM2S), B4GalT1 (B4G1), and MGAT1 in addition to Gb3S) were expressed in ΔLAPTM4A/LAPTM4A-HA cells to examine their interaction with LAPTM4A-HA using anti-NeonGreen beads. LAPTM4A-HA immunoprecipitated with Gb3S-NG much more than with the other tested glycosyltransferase (GT)-NGs, suggesting that LAPTM4A preferentially interacted with Gb3S (Figure 5C). Interestingly, an upper band (≈23kDa), but no lower band (≈18kDa), co-immunoprecipitated with Gb3S-NG. The band of HA-LAPTM4A was observed only at 23 kDa (Figure 5B), which is the same as the upper band of LAPTM4A-HA, suggesting that LAPTM4A-HA in the lower band may have been an N-terminal truncation form. Therefore, LAPTM4A may interact with Gb3S at its N-terminal region.

Human LAPTM4A has 46% amino acid homology with human LAPTM4B, another LAPTM family member involved in tumor progression (Meng et al., 2016) and lysosomal ceramide transport (Blom et al., 2015) (Figure 4A). However, LAPTM4B did not compensate for the reduction of Gb3 due to LAPTM4A deficiency (Figures 4B–4D), indicating that the molecular activity of LAPTM4B differs from that of LAPTM4A.

Molecular Assessment of TM9SF2 Regulation of the Gb3 Synthesis

TM9SF2 is a member of the TM9SF family characterized by nine transmembrane domains, with four reported family members (TM9SF1-4) in mammals (Figure 6A) (Chluba-de Tapia et al., 1997; Schimmöller

et al., 1998; Lozupone et al., 2009). However, the functional similarity of these proteins is currently unknown. Therefore, we examined whether TM9SF1, 3, or 4 was able to compensate for the loss of TM9SF2 using transient transfection of these cDNAs into *TM9SF2*-KO cells. Expression of TM9SF1–4 was confirmed at the transcriptional level (Figure 6B for TM9SF1, 3, and 4) or at the translation level (Figure 6C for TM9SF2). Fluorescence-activated cell sorting (FACS) analysis revealed that all TM9SFs restored STx binding in *TM9SF2*-KO cells, indicating that regulation of Gb3 synthesis is conserved among TM9SF family members (Figure 6D). The effect of disrupting these TM9SF gene homologs on Gb3 synthesis was then investigated. Transfection of sgRNA targeting to TM9SF2 as well as Gb3S (A4GalT) reduced STx surface binding, whereas sgRNAs targeting other TM9SFs, and a combination of sgRNAs targeting other family members, did not reduce STx binding, although mutations of *TM9SF1*, *3*, and *4* genes occurred as often as that of the *TM9SF2* gene (Figures S5A and S5B). These results indicated that TM9SF2 was the predominant Gb3 regulator among the TM9SF family members, at least in HeLa cells.

TM9SF family proteins have a consensus KxD/E motif (KVD in TM9SF2) at the C terminus, which interacts with the COPI coatomer. In TM9SF family proteins, C-terminal tagging, which masks the terminus, or mutation of the motif, affects interaction with COPI and subcellular localization (Woo et al., 2015). Therefore, we examined whether the C-terminal KxD/E motif of TM9SF2 was required for regulation of Gb3 synthesis. Transfection of C-terminal HA-tagged TM9SF2 (TM9SF2-HA) did not restore STx binding in *TM9SF2*-KO cells (Figure 6D). However, western blot analysis revealed that full-length TM9SF2-HA was not present for unknown reasons (Figure 6C). Therefore, we mutated the C-terminal KxD/E motif (KVD to SVN or AVA) or deleted the motif (CΔ3). These mutations reduced restoration of Gb3 synthesis in *TM9SF2*-KO cells, and CΔ3 resulted in complete loss of this activity, despite expression at levels equivalent to that of wild-type TM9SF2 (Figures 6C and 6D). These results indicated that the C terminus of TM9SF2 is required for the regulation of Gb3 synthesis.

To investigate the interaction between TM9SF2 and Gb3S, an HA-tag was inserted following the putative signal peptide in TM9SF2 (spHA-TM9SF2) (Figure S6A). The spHA-TM9SF2 maintained the ability to restore Gb3 synthesis in *TM9SF2*-KO cells, whereas deletion of the three C-terminal amino acids ablated this ability (Figure S6B). TM9SF2 is known to be localized at the Golgi (Tanaka et al., 2017; Pacheco et al., 2018). However, Golgi localization of spHA-TM9SF2 as well as spHA-TM9SF2 CΔ3 was decreased, although the reason for these differences is unknown (Figure S6C). In this condition, immunoprecipitation analysis using anti-HA agarose beads demonstrated that the high mannose type of Gb3 synthase specifically co-immunoprecipitated with spHA-TM9SF2 and spHA-TM9SF2 CΔ3 but not with GRINA TM4-6-HA, which is a previously reported negative control (Yamaji et al., 2010) (Figure S6D). The selective interaction of high mannose type Gb3 synthase may be due to the localization of spHA-TM9SF2, where only the high mannose type Gb3 synthase was localized. Future studies will clarify whether the interaction with high mannose type Gb3 synthase is specific, or rather is an as yet unidentified artifact. However, taken together, these results suggest that TM9SF2 could interact with Gb3 synthase. Next, spHA-TM9SF2 was transfected into several GT-NG-expressing cell lines to examine their interaction with spHA-TM9SF2. spHA-TM9SF2 immunoprecipitated with Gb3S-NG but did not robustly immunoprecipitate with other GT-NGs, suggesting that TM9SF2 selectively bound Gb3 synthase (Figure S6E).

TM9SF2 Regulation of Gb3 Synthase Subcellular Localization

As demonstrated earlier, TM9SF2 did not affect the amount or activity of endogenous Gb3 synthase. One hypothesis is that Gb3 synthase may not be able to encounter its substrates in *TM9SF2*-KO cells because of membrane transport defects. Several reports indicated that Gb3 synthase is mainly localized to the TGN rather than to the Golgi cisternae (Yamaji et al., 2010; D'Angelo et al., 2013). Therefore, the intracellular distribution of endogenous TGN46, a TGN marker, was first examined (Figure S7). In parent cells and *LAPTM4A*-KO cells, most TGN46 proteins were merged or aligned with GM130, a cis/medial Golgi marker, whereas in *TM9SF2*-KO cells, more than 30% of cells included dispersed punctate TGN46 staining, which was not merged with GM130. The disruption of TGN46 distribution was restored by expression of TM9SF2. These data suggested that TM9SF2 affected transport of TGN membranes.

To assess the effect of TM9SF2 on intracellular localization of Gb3 synthase, Gb3S-NG was expressed in *TM9SF2*-KO cells (ΔTM9SF2/Gb3S-NG) and TM9SF2-rescued cells (ΔTM9SF2/TM9SF2/Gb3S-NG) (Figure S4). Western blot analysis revealed that the expression level of Gb3S-NG was similar among these

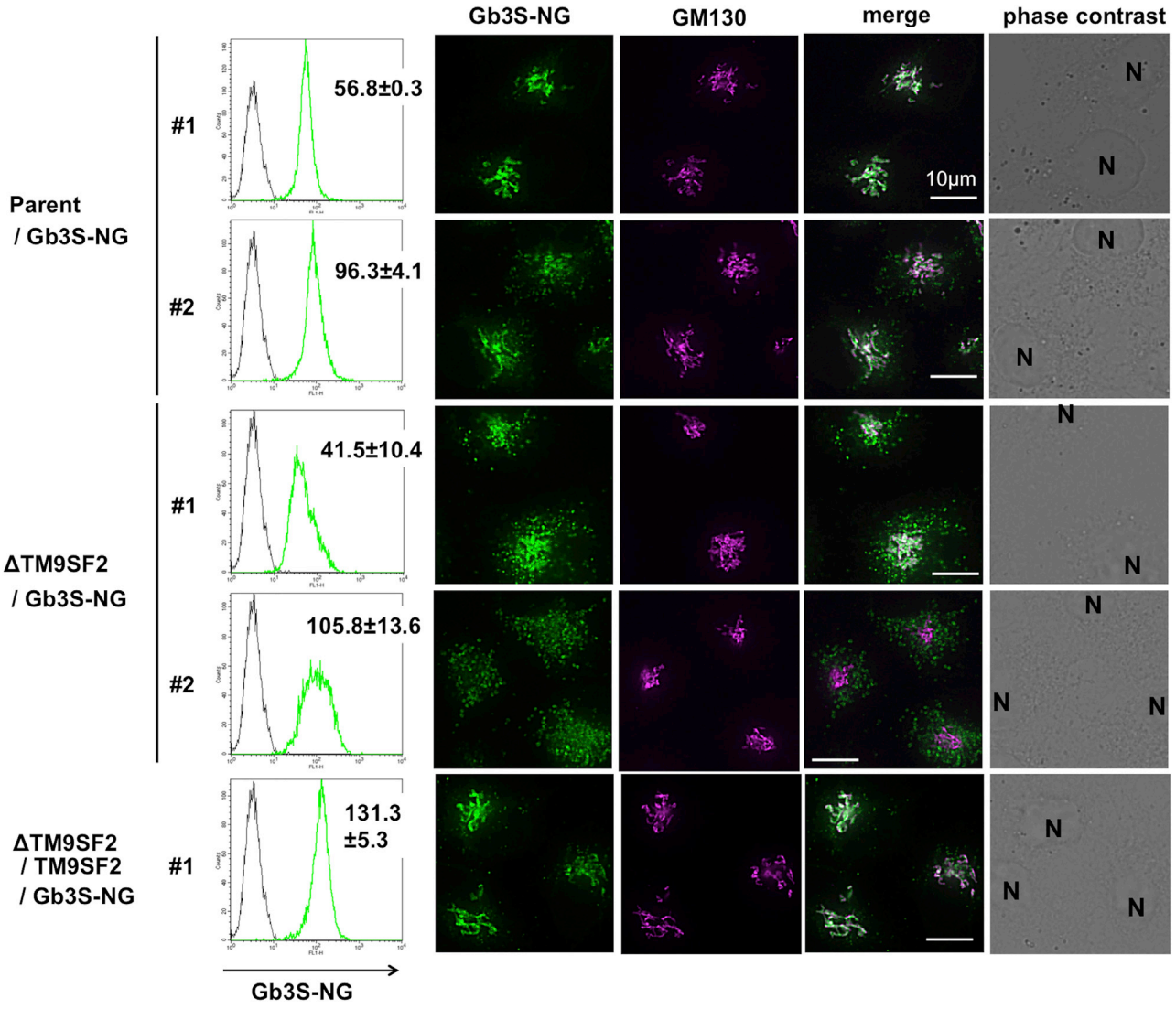

Figure 7. Intracellular Distribution of Exogenously Expressed Gb3S-moxNeonGreen is Disrupted in *TM9SF2*-KO Cells

Dispersed punctate structures of Gb3S-moxNeonGreen (NG) in KO cells. Two parent cell clones expressing different levels of Gb3S-NG proteins, two *TM9SF2*-KO cell clones expressing different levels of Gb3S-NG proteins, and a TM9SF2-complemented cell clone expressing higher levels of Gb3S-NG proteins were stained with anti GM130 (Golgi), shown in magenta. Scale bars, 10 μm. Level of exogenously expressed Gb3S-NG in the indicated cell clones was determined by FACS analysis (yellow-green line, the mean ± SD obtained from three independent experiments).
See also Figures S4 and S7–S9.

cell lines, and truncation of Gb3S-NG was not observed, suggesting that the fluorescent signal was indicative of full-length Gb3S-NG (Figure S4A). Compared with parent cells, most *TM9SF2*-KO cells contained punctate staining of Gb3S-NG around the Golgi, although the degree of dispersion varied depending on the expression level of Gb3S-NG (Figure S4B). To compare the localization of Gb3 synthase at the same expression level, several clones with different expression levels of Gb3S-NG were isolated. In Gb3S-NG-expressing parent cell clones, most Gb3S-NG proteins were co-localized with or aligned with the Golgi marker GM130 (clone #1), and when the expression level of Gb3S-NG was higher (clone #2, mean fluorescent intensity [MFI] 96.3 compared with MFI 56.8 in clone #1), slight punctate staining appeared around the Golgi (Figure 7). Contrastingly, in Gb3S-NG-expressing *TM9SF2* KO cell clones, more intense punctate staining was observed despite lower expression of Gb3S-NG (clone #1, MFI 41.5), and when the expression of Gb3S-NG was high (clone #2, MFI 105.8), punctate staining was further dispersed. The dispersed punctate staining diminished in Gb3S-NG-expressing TM9SF2-rescued cells, even when the expression of

Gb3S-NG was higher in rescued cells (MFI 131.3) than that of Gb3S-NG-expressing KO cell clone #2 (MFI 105.8). These results suggested that TM9SF2 was required for proper Golgi/TGN localization of Gb3 synthase. Unlike TM9SF2, disruption of other TM9SFs (1, 3, and 4) did not affect localization of Gb3S (Figure S5C). On the other hand, intracellular localizations of other GT-NG fusion proteins (B4GalT5, GM2 synthase, B4GalT1, and MGAT1) were also likely perturbed in *TM9SF2*-KO cells (Figure S8). Therefore, the effect of TM9SF2 on transport of Golgi-resident enzymes may be greater than expected, although the effect of glycan metabolism has not yet been examined.

Next, we determined which organelle markers were co-localized with the punctate structures of Gb3S-NG in *TM9SF2*-KO cells (Figure S9). Most punctate dots of Gb3S-NG co-localized with TGN46, a TGN marker protein, but not GM130, a *cis/medial*-Golgi marker protein, suggesting that Gb3 synthase was mislocalized together with TGN46. These Gb3S-NG punctate structures were not completely merged with late endosome markers Rab7 and Rab9 and the lysosomal marker LAMP2 but seemed to be in contact with these markers. On the other hand, EEA1, an early endosome marker, did not co-localize with Gb3S-NG punctate structures. Some TGN proteins, including TGN46, are known to be cycled between the TGN, plasma membrane, and endosomes (Ladinsky and Howell, 1992; Pfeffer, 2011). Therefore, as a hypothesis, Gb3 synthase may also cycle between the TGN and endosomes and TM9SF2 may be required for retrograde transport of Gb3 synthase to the TGN/Golgi, which should be clarified in future.

DISCUSSION

GSL biosynthesis is regulated by a number of factors, but changes in lipid composition have primarily been ascribed to transcriptional regulation of glycosyltransferases. To take an unbiased approach toward identifying novel regulatory mechanisms, we used a genome-wide CRISPR library screen for STx-induced cell death in HeLa cells to demonstrate that various genes, including sphingolipid-related genes and membrane trafficking genes, were comprehensively enriched. In addition, we identified two previously uncharacterized genes, *LAPTM4A* and *TM9SF2*, which were essential for STx binding and subsequent STx cytotoxicity.

Previously, several genome-wide RNAi and CRISPRi screens using STx and cholera toxin, which is another GSL-binding toxin, have been reported (Guimaraes et al., 2011; Gilbert et al., 2014; Selyunin et al., 2017). In genetic screens utilizing toxin-induced cell death, the identified factors may be broadly categorized into two functional groups, comprising genes regulating retrograde trafficking of toxins from the plasma membrane to the ER and cytosol or genes regulating GSL biosynthesis or GSL-synthesizing enzymes. The above-mentioned studies focused primarily on retrograde toxin transport or development of the screening systems. Contrastingly, GSL metabolism has not been well investigated, prompting us to perform the present screen. Some identified genes in our screen were also enriched in prior screens, including *UNC50* (Gilbert et al., 2014; Selyunin et al., 2017) and *TM9SF2* (Gilbert et al., 2014), whereas the GET complex (*GET4* and *CAMLG*, described later) was first observed in this screen.

Just before submission of this manuscript, another group also reported that loss of *LAPTM4A* and *TM9SF2* disrupted STx cell surface binding but did not address the mechanism of action, including the effect of these proteins on Gb3 biosynthesis (Pacheco et al., 2018). We further analyzed the molecular mechanisms for LAPTM4A and TM9SF2 regulation of STx sensitivity using biochemical and cell biology assays. Cumulatively, we demonstrated the following: (1) both LAPTM4A and TM9SF2 were required for Gb3 biosynthesis from LacCer, catalyzed by Gb3 synthase; (2) LAPTM4A and TM9SF2 had differential mechanisms of action, as disruption of LAPTM4A, but not TM9SF2, reduced endogenous Gb3 synthase activity; (3) LAPTM4A and TM9SF2 interacted with Gb3 synthase; (4) ablation of TM9SF2 disrupted the localization of Gb3 synthase; and (5) regulation of Gb3 is conserved in TM9SF family members, and the C-terminus of the proteins is essential for this activity.

The molecular and physiological roles of LAPTM4A remain incompletely understood. Several reports demonstrated that LAPTM4A is mainly localized to lysosomes and late endosomes, at least when it was overexpressed (Cabrita et al., 1999; Hogue et al., 2002; Grabner et al., 2011), which was consistent with our results (Figures 4E and S3). A previous report identified that overexpression of LAPTM4A decreased cell surface localization of OST2 proteins, instead recruiting these proteins to endocytic compartments (Grabner et al., 2011). Another report used genome-wide RNAi screening to identify LAPTM4A as a potential regulator of endosome-to-Golgi retrieval, although a functional analysis was not conducted (Breusegem and Seaman, 2014). LAPTM4A has a cytoplasmic region required for lysosomal sorting through

NEDD4 binding (Hogue et al., 2002; Milkereit and Rotin, 2011), but the present study demonstrated that this region is dispensable for LAPTM4A regulation of Gb3 synthesis. Interestingly, C-terminal deletion mutant proteins (LAPTM4AΔC-HA) were mainly localized to the ER (Figure 4E), whereas Gb3 synthase is mainly localized to the TGN. We carefully observed localization of LAPTM4A-HA, HA-LAPTM4A, and LAPTM4AΔC-HA proteins, and all proteins were partially localized to the Golgi apparatus (Figures 4E and S3). Furthermore, LAPTM4A-HA staining at the Golgi was increased by overexpression of Gb3 synthase (Gb3S-NG) (Figure 5A), and LAPTM4A interacted with Gb3 synthase, as demonstrated by immunoprecipitation analysis (Figures 5B and 5C). One potential explanation for these results is that LAPTM4A may cycle between endosome and the Golgi and a small amount of LAPTM4A in the Golgi may be sufficient to localize Gb3 synthase to the TGN/Golgi to regulate its activity or prevent its degradation.

Unfortunately, we were unable to find an anti-Gb3 synthase antibody capable of detecting endogenous Gb3 synthase in western blots and immunofluorescent staining. It is therefore unclear whether decreased Gb3 synthase activity in *LAPTM4A*-KO cells was due to reduction in the amount of Gb3 synthase proteins through synthesis inhibition or degradation or instead was due to inhibition of Gb3 synthase activity without reduction in protein levels. We examined whether loss of LAPTM4A affected the abundance of exogenous Gb3 synthase and found that abundance of exogenous Gb3 synthase was not changed in *LAPTM4A*-KO cells relative to parent cells (Figure S2G). However, this result may not be reflective of endogenous Gb3 synthase regulation, and the ability to detect endogenous Gb3 synthase will better clarify this regulatory mechanism, which will be the topic of future investigations.

LAPTM4B is a paralog of LAPTM4A and has 44% amino acid identity and 63% amino acid similarity. Furthermore, LAPTM4B is also localized to lysosomes and late endosomes through NEDD4 binding. LAPTM4B is known to promote growth of tumor cells and function as a lysosomal ceramide exporter (Blom et al., 2015; Meng et al., 2016). However, there were no prior reports addressing functional similarity between these proteins. We demonstrated in the present study that LAPTM4B did not complement the Gb3 regulatory function of LAPTM4A, suggesting that LAPTM4A has a paralog-specific function that may be related to its multispanning transmembrane domains, which are not conserved in LAPTM4B (Figure 4D). Mutational analyses assessing differential domains between these two proteins will further elucidate the function of LAPTM4A.

Contrary to LAPTM4A, loss of TM9SF2 did not change Gb3 synthase activity *in vitro* despite decreased cellular Gb3 biosynthesis. This suggested that loss of TM9SF2 did not change the protein abundance of Gb3 synthase but instead regulated Gb3 synthase proximity to its substrates, LacCer and UDP-galactose, in intact cells. Gb3S-NG fusion proteins were localized to the Golgi/TGN in parent cells, but in *TM9SF2*-KO cells, Gb3 synthase localization was disrupted, appearing in punctate structures localized with the TGN marker TGN46. Pacheco et al. demonstrated that the localization of both endogenous Gb3S and TGN46 were unchanged in *TM9SF2*-KO cells (Pacheco et al., 2018), which is inconsistent with our results. The reason for this discrepancy is unknown, but it could be due to limitations of endogenous Gb3 synthase. As described earlier, we could not detect a specific signal for endogenous Gb3 synthase by comparison of parent cells with *Gb3S*-KO cells, and it was hard to compare such a low expression level of Gb3 synthase (Figure S2). Instead, we demonstrated that, in addition to the localization of exogenous Gb3 synthase, localization of endogenous TGN46, which was co-localized or aligned with GM130 in parent cells, was also affected in *TM9SF2*-KO cells and that this alteration was restored by overexpression of wild-type TM9SF2 (Figure S7). Taken together with the result that TM9SF2 interacts with Gb3 synthase (Figures S6D and S6E), we suggest that TM9SF2 regulates transport of Gb3 synthase. The punctate Gb3 synthase structures were proximal to late endosomes and lysosomes, suggesting capture by late endosomes/lysosomes (Figure S9). The dynamics of Gb3 synthase transport have not yet been elucidated, but Gb3 synthase may be transported between the TGN and endosomes, and loss of TM9SF2 may affect retrograde transport of Gb3 synthase. Punctate localization of Gb3 synthase was also observed in our prior study, when TMBIM family molecules were overexpressed and Gb3 was decreased (Yamaji et al., 2010). Therefore, perturbed distribution of Gb3 synthase in *TM9SF2*-KO cells may explain the subsequent decrease in Gb3 synthesis, as mislocalization of Gb3 synthase and subsequent decreases of LacCer substrate availability would disrupt Gb3 biosynthesis despite unchanged total abundance of Gb3 synthase.

A recent study demonstrated that TM9SF2 is required for the expression of bifunctional heparan sulfate N-deacetylase/N-sulfotransferase 1 (NDST1), which is involved in heparan sulfate biosynthesis, and that loss of TM9SF2 caused defective heparan sulfate synthesis in a HAP1 haploid cell line (Tanaka et al., 2017). In this

case, exogenously expressed NDST1 was decreased in *TM9SF2*-KO HAP1 cells. In contrast, in the present study, loss of TM9SF2 did not change the expression of Gb3S-NG in HeLa cells (Figure S4A). This discrepancy may be due to the difference in enzymes used as substrates, potentially due to differences in cell types.

Previous reports demonstrated that TM9SF2 is primarily localized to the Golgi (Woo et al., 2015; Tanaka et al., 2017). The C-terminal region of TM9SF2 is thought to bind COPI coat proteins, which is important for the localization of TM9SF2 (Woo et al., 2015). Our study demonstrated that the C-terminal region of TM9SF2 was functionally important, as HA-tagging the C-terminus or targeted deletion or mutation of the last three amino acids resulted in loss of the Gb3 regulatory activity of TM9SF2. COPI vesicles are important for intra-Golgi and Golgi-ER retrograde transport (Lee et al., 2004; Yang et al., 2011). Consistent with this mechanism, COPE-targeting sgRNA, which codes the COPI coatomer subunit ε, was also enriched in this screen, although the fold enrichment was low (Figure 1A). However, this also supports the notion that retrograde transport of TM9SF2 is important for its function. The GSL biosynthesis pattern in *TM9SF2*-KO cells differed slightly from that of *LAPTM4A*-KO cells. In *LAPTM4A*-KO cells, the reduction of Gb3 corresponded with increased levels of its direct precursor LacCer, suggesting that LAPTM4A specifically affected Gb3 synthase. In contrast, *TM9SF2*-KO cells had only a modest increase in LacCer, and GlcCer was also modestly increased (Figures 2E and 2F). This suggests that TM9SF2 may affect not only Gb3 synthase but also other glycosyltransferases. Disturbed localization of various glycosyltransferases in *TM9SF2*-KO cells may account for the observed phenotype, which should be addressed in future studies (Figure S8).

TM9SF2 has three paralogs, TM9SF1 (31% amino acid identity and 49% amino acid similarity), TM9SF3 (31%, 49%), and TM9SF4 (44%, 62%). The respective functions of each TM9SF family member have been previously reported (Bergeret et al., 2008; He et al., 2009; Oo et al., 2014), but conserved activity among family members has not been extensively investigated. The present study demonstrated that all TM9SF family proteins potentially had the same regulatory activity of Gb3 biosynthesis, although the amino acid identity is only 31%. Detailed analyses of conserved amino acids and functional domains among family members will contribute to understanding the molecular machinery of the TM9SF family. On the other hand, disruption of TM9SF1, 3, and 4 did not affect synthesis of Gb3 and localization of Gb3 synthase. This is consistent with the result that only TM9SF2 was enriched in this screening. The quantitative subcellular proteomic analysis referenced earlier demonstrated that all TM9SF family proteins are expressed at similar levels in HeLa cells (Itzhak et al., 2016). Therefore, the Gb3-regulating activity of TM9SF1, 3, and 4 may be less than that of TM9SF2 at endogenous expression levels.

In addition to sphingolipid enzyme genes, various membrane trafficking genes, especially those involved in retrograde transport, were enriched in the screen. Some of these genes, including COG complex, GARP complex, *UNC50*, and *PTAR1*, a putative prenyltransferase for small G proteins, were also enriched in several other genome-wide screens related to proteoglycans (Rift Valley fever virus [Riblett et al., 2015] and Chikungunya virus [Tanaka et al., 2017]), glycoproteins (Ricin [Bassik et al., 2013] and Lassa virus [Jae et al., 2013, 2014]), and glycolipids (cholera toxin [Gilbert et al., 2014] as well as STx [Selyunin et al., 2017]). Previous studies have identified that the COG complex and GARP complex are involved in toxin trafficking and that depletion of these proteins compromises trafficking (Zolov and Lupashin, 2005; Bailey Blackburn et al., 2016; Pérez-Victoria et al., 2008). Recent screening studies indicate that these membrane trafficking genes more generally affect glycosylation, likely through retrograde trafficking defects of glycosyltransferases, which may overlap with retrograde trafficking of toxins. Loss of the GET complex leads to mislocalization of tail-anchored proteins, including syntaxins involved in retrograde transport (Norlin et al., 2016), which may be why the GET complex was isolated in this screen. The genes identified in this screen have not been fully analyzed, and comparison of GSL biosynthesis in KO or knockdown cells will clarify the functional interactions between genes, and the relationship between these factors and glycosylation, which is a subject of future investigations.

During the second revision process of this manuscript, Tian S. et al. published a similar work demonstrating that disruption of LAPTM4A and TM9SF2 reduced Gb3 (Tian et al., 2018). The authors demonstrated that loss of LAPTM4A did not change the expression level of endogenous Gb3 synthase. Together with our data that loss of LAPTM4A reduced Gb3 synthase activity *in vitro*, LAPTM4A may regulate Gb3 synthase activity, rather than reduce the amount of Gb3 synthase.

In summary, we performed a genome-wide loss-of-function screen using a CRISPR library to identify genes that conferred resistance to STx1. Among the enriched genes, we identified two factors, TM9SF2 and

LAPTM4A, which post-transcriptionally regulated Gb3 synthase through differential mechanisms. Furthermore, the Gb3-regulating activity of TM9SF2 is conserved among other TM9SF family proteins, although TM9SF2 is the predominant Gb3 regulator among the family proteins in HeLa cells. These results provide mechanistic insight into post-translational regulation of Gb3 synthase activity and localization.

Limitations of the Study

In this study, we found that loss of LAPTM4A reduced Gb3 synthase activity. Therefore, measurement of endogenous Gb3S protein level in *LAPTM4A* KO cells is important to understand the function of LAPTM4A. We attempted to detect endogenous Gb3 synthase proteins using antibodies against Gb3 synthase. However, unfortunately, we were unable to find an anti-Gb3 synthase antibody capable of detecting endogenous Gb3 synthase in western blots and immunofluorescent staining using parent cells, *Gb3S*-KO cells, and Gb3S-overexpressing cells, although one of three commercially available antibodies clearly detected exogenously expressed Gb3 synthase in both methods (Figures S2A–S2D). In a recent quantitative subcellular proteomic analysis of Gb3 synthase localization, endogenous Gb3 synthase was still below the detection limit in HeLa cells, although approximately 9,000 proteins were detected, including glucosylceramide synthase (UGCG) and lactosylceramide synthase (B4GalT5) (Itzhak et al., 2016). We also demonstrated that the expression level of endogenous Gb3 synthase was less than 1% of exogenously expressed Gb3 synthase (Figure S2C) and HA-tagged Gb3S at an endogenous expression level was only slightly detected when Gb3S-HA was immunoprecipitated, in an analysis using HA-tag knock-in cells (Figures S2E and S2F). These results indicate that the expression level of endogenous Gb3 synthase is quite low. Most overexpressed Gb3 synthase proteins are glycosylated with either high-mannose type or complex type N-glycans in HeLa cells (Figure S2), and it is likely important to distinguish between the two glycosylation types of Gb3 synthase in considering the dynamics of Gb3 synthase (Yamaji et al., 2010). Therefore, the ability to detect both types of endogenous Gb3 synthase quantitatively will better clarify this regulatory mechanism, which will be the topic of future investigations.

METHODS

All methods can be found in the accompanying Transparent Methods supplemental file.

DATA AND SOFTWARE AVAILABILITY

The sgRNA data reported in this study have been deposited to the NCBI GEO and are available under accession number GEO: GSE116730.

SUPPLEMENTAL INFORMATION

Supplemental Information includes Transparent Methods, nine figures, and three data files and can be found with this article online at https://doi.org/10.1016/j.isci.2018.12.039.

ACKNOWLEDGMENTS

This work was supported by the JSPS KAKENHI (No. JP26440069 and No. JP17K07357 to T.Y.), MEXT KAKENHI (No. JP17H06417 to K.H.), AMED J-PRIDE (No. JP18fm0208005j0102 to T.Y. and No. JP18fm0208005j0202 to T.S.), AMED CREST (No. JP18gm0910005 to K.H.), and Mizutani Foundation for Glycoscience (No. 160123 to T.Y.).

AUTHOR CONTRIBUTIONS

Conceptualization, T.Y.; Investigation, T.Y., T.S., Y.T., C.S., and K.M.; Data Analysis, T.Y., T.S., M.K., and K.H.; Writing, T.Y. and K.H.; Funding Acquisition, T.Y., T.S, and K.H.

DECLARATION OF INTERESTS

The authors declare no competing interests.

Received: July 20, 2018
Revised: November 13, 2018
Accepted: December 28, 2018
Published: January 25, 2019

REFERENCES

Bailey Blackburn, J., Pokrovskaya, I., Fisher, P., Ungar, D., and Lupashin, V.V. (2016). COG complex complexities: detailed characterization of a complete set of HEK293T cells lacking individual COG subunits. Front. Cell Dev. Biol. *4*, 23.

Bassik, M.C., Kampmann, M., Lebbink, R.J., Wang, S., Hein, M.Y., Poser, I., Weibezahn, J., Horlbeck, M.A., Chen, S., Mann, M., et al. (2013). A systematic mammalian genetic interaction map reveals pathways underlying ricin susceptibility. Cell *152*, 909–922.

Bergeret, E., Perrin, J., Williams, M., Grunwald, D., Engel, E., Thevenon, D., Taillebourg, E., Bruckert, F., Cosson, P., and Fauvarque, M.O. (2008). TM9SF4 is required for Drosophila cellular immunity via cell adhesion and phagocytosis. J. Cell Sci. *121*, 3325–3334.

Blackburn, J.B., and Lupashin, V.V. (2016). Creating knockouts of conserved oligomeric golgi complex subunits using CRISPR-mediated gene editing paired with a selection strategy based on glycosylation defects associated with impaired COG complex function. Methods Mol. Biol. *1496*, 145–161.

Blom, T., Li, S., Dichlberger, A., Bäck, N., Kimm, Y.A., Loizides-Mangold, U., Riezman, H., Bittman, R., and Ikonen, E. (2015). LAPTM4B facilitates late endosomal ceramide export to control cell death pathways. Nat. Chem. Biol. *11*, 799–806.

Bonifacino, J.S., and Hierro, A. (2011). Transport according to GARP: receiving retrograde cargo at the trans-Golgi network. Trends. Cell Biol. *21*, 159–167.

Breusegem, S.Y., and Seaman, M.N.J. (2014). Genome-wide RNAi screen reveals a role for multipass membrane proteins in endosome-to-Golgi retrieval. Cell Rep. *9*, 1931–1945.

Cabrita, M.A., Hobman, T.C., Hogue, D.L., King, K.M., and Cass, C.E. (1999). Mouse transporter protein, a membrane protein that regulates cellular multidrug resistance, is localized to lysosomes. Cancer Res. *59*, 4890–4897.

Chluba-de Tapia, J., de Tapia, M., Jäggin, V., and Eberle, A.N. (1997). Cloning of a human multispanning membrane protein cDNA: evidence for a new protein family. Gene *197*, 195–204.

Clarke, J.T. (2007). Narrative review: Fabry disease. Ann. Intern. Med. *146*, 425–433.

Costantini, L.M., Baloban, M., Markwardt, M.L., Rizzo, M., Guo, F., Verkhusha, V.V., and Snapp, E.L. (2015). A palette of fluorescent proteins optimized for diverse cellular environments. Nat. Commun. *6*, 7670.

D'Angelo, G., Uemura, T., Chuang, C.C., Polishchuk, E., Santoro, M., Ohvo-Rekilä, H., Sato, T., Di Tullio, G., Varriale, A., D'Auria, S., et al. (2013). Vesicular and non-vesicular transport feed distinct glycosylation pathways in the Golgi. Nature *501*, 116–120.

Gilbert, L.A., Horlbeck, M.A., Adamson, B., Villalta, J.E., Chen, Y., Whitehead, E.H., Guimaraes, C., Panning, B., Ploegh, H.L., Bassik, M.C., et al. (2014). Genome-scale CRISPR-mediated control of gene repression and activation. Cell *159*, 647–661.

Grabner, A., Brast, S., Sucic, S., Bierer, S., Hirsch, B., Pavenstädt, H., Sitte, H.H., Schlatter, E., and Ciarimboli, G. (2011). LAPTM4A interacts with hOCT2 and regulates its endocytotic recruitment. Cell. Mol. Life Sci. *68*, 4079–4090.

Guimaraes, C.P., Carette, J.E., Varadarajan, M., Antos, J., Popp, M.W., Spooner, E., Brummelkamp, T.R., and Ploegh, H.L. (2011). Identification of host cell factors required for intoxication through use of modified cholera toxin. J. Cell Biol. *195*, 751–764.

Hakomori, S.I. (2008). Structure and function of glycosphingolipids and sphingolipids: recollections and future trends. Biochim. Biophys. Acta *1780*, 325–346.

Han, G., Gupta, S.D., Gable, K., Niranjanakumari, S., Moitra, P., Eichler, F., Brown, R.H., Jr., Harmon, J.M., and Dunn, T.M. (2009). Identification of small subunits of mammalian serine palmitoyltransferase that confer distinct acyl-CoA substrate specificities. Proc. Natl. Acad. Sci. U S A *106*, 8186–8191.

Hanada, K., Kumagai, K., Yasuda, S., Miura, Y., Kawano, M., Fukasawa, M., and Nishijima, M. (2003). Molecular machinery for non-vesicular trafficking of ceramide. Nature *426*, 803–809.

Hanada, K. (2005). Sphingolipids in infectious diseases. Jpn. J. Infect. Dis. *58*, 131–148.

He, P., Peng, Z., Luo, Y., Wang, L., Yu, P., Deng, W., An, Y., Shi, T., and Ma, D. (2009). High-throughput functional screening for autophagy-related genes and identification of TM9SF1 as an autophagosome-inducing gene. Autophagy *5*, 52–60.

Hogue, D.L., Nash, C., Ling, V., and Hobman, T.C. (2002). Lysosome-associated protein transmembrane 4 alpha (LAPTM4 alpha) requires two tandemly arranged tyrosine-based signals for sorting to lysosomes. Biochem. J. *365*, 721–730.

Ichikawa, S., Sakiyama, H., Suzuki, G., Hidari, K.I., and Hirabayashi, Y. (1996). Expression cloning of a cDNA for human ceramide glucosyltransferase that catalyzes the first glycosylation step of glycosphingolipid synthesis. Proc. Natl. Acad. Sci. U S A *93*, 4638–4643.

Itzhak, D.N., Tyanova, S., Cox, J., and Borner, G.H. (2016). Global, quantitative and dynamic mapping of protein subcellular localization. Elife *5*, e16950.

Jae, L.T., Raaben, M., Herbert, A.S., Kuehne, A.I., Wirchnianski, A.S., Soh, T.K., Stubbs, S.H., Janssen, H., Damme, M., Saftig, P., et al. (2014). Virus entry. Lassa virus entry requires a trigger-induced receptor switch. Science *344*, 1506–1510.

Jae, L.T., Raaben, M., Riemersma, M., van Beusekom, E., Blomen, V.A., Velds, A., Kerkhoven, R.M., Carette, J.E., Topaloglu, H., Meinecke, P., et al. (2013). Deciphering the glycosylome of dystroglycanopathies using haploid screens for Lassa virus entry. Science *340*, 479–483.

Kojima, Y., Fukumoto, S., Furukawa, K., Okajima, T., Wiels, J., Yokoyama, K., Suzuki, Y., Urano, T., Ohta, M., and Furukawa, K. (2000). Molecular cloning of globotriaosylceramide/CD77 synthase, a glycosyltransferase that initiates the synthesis of globo series glycosphingolipids. J. Biol. Chem. *275*, 15152–15156.

Kondo, Y., Ikeda, K., Tokuda, N., Nishitani, C., Ohto, U., Akashi-Takamura, S., Ito, Y., Uchikawa, M., Kuroki, Y., Taguchi, R., et al. (2013). TLR4-MD-2 complex is negatively regulated by an endogenous ligand, globotetraosylceramide. Proc. Natl. Acad. Sci. U S A *110*, 4714–4719.

Kovbasnjuk, O., Mourtazina, R., Baibakov, B., Wang, T., Elowsky, C., Choti, M.A., Kane, A., and Donowitz, M. (2005). The glycosphingolipid globotriaosylceramide in the metastatic transformation of colon cancer. Proc. Natl. Acad. Sci. U S A *102*, 19087–19092.

Kumagai, T., Sato, T., Natsuka, S., Kobayashi, Y., Zhou, D., Shinkai, T., Hayakawa, S., and Furukawa, K. (2010). Involvement of murine β-1,4-galactosyltransferase V in lactosylceramide biosynthesis. Glycoconj. J. *27*, 685–695.

Ladinsky, M.S., and Howell, K.E. (1992). The trans-Golgi network can be dissected structurally and functionally from the cisternae of the Golgi complex by brefeldin A. Eur. J. Cell Biol. *59*, 92–105.

Lee, M.C., Miller, E.A., Goldberg, J., Orci, L., and Schekman, R. (2004). Bi-directional protein transport between the ER and Golgi. Annu. Rev. Cell Dev. Biol. *20*, 87–123.

Lozupone, F., Perdicchio, M., Brambilla, D., Borghi, M., Meschini, S., Barca, S., Marino, M.L., Logozzi, M., Federici, C., Iessi, E., et al. (2009). The human homologue of *Dictyostelium discoideum* phg1A is expressed by human metastatic melanoma cells. EMBO Rep. *10*, 1348–1354.

Meng, Y., Wang, L., Chen, D., Chang, Y., Zhang, M., Xu, J.J., Zhou, R., and Zhang, Q.Y. (2016). LAPTM4B: an oncogene in various solid tumors and its functions. Oncogene *35*, 6359–6365.

Milkereit, R., and Rotin, D. (2011). A role for the ubiquitin ligase Nedd4 in membrane sorting of LAPTM4 proteins. PLoS One *6*, e27478.

Norlin, S., Parekh, V.S., Naredi, P., and Edlund, H. (2016). Asna1/TRC40 controls β-cell function and endoplasmic reticulum homeostasis by ensuring retrograde transport. Diabetes *65*, 110–119.

Oo, H.Z., Sentani, K., Sakamoto, N., Anami, K., Naito, Y., Oshima, T., Yanagihara, K., Oue, N., and Yasui, W. (2014). Identification of novel transmembrane proteins in scirrhous-type gastric cancer by the *Escherichia coli* ampicillin secretion trap (CAST) method: TM9SF3 participates in tumor invasion and serves as a prognostic factor. Pathobiology *81*, 138–148.

Pacheco, A.R., Lazarus, J.E., Sit, B., Schmieder, S., Lencer, W.I., Blondel, C.J., Doench, J.G., Davis, B.M., and Waldor, M.K. (2018). CRISPR screen reveals that EHEC's T3SS and shiga toxin rely on shared host factors for infection. MBio *9*, e01003–01018.

Pérez-Victoria, F.J., Mardones, G.A., and Bonifacino, J.S. (2008). Requirement of the human GARP complex for mannose 6-phosphate-receptor-dependent sorting of cathepsin D to lysosomes. Mol. Biol. Cell *19*, 2350–2362.

Pfeffer, S.R. (2011). Entry at the trans-face of the Golgi. Cold Spring Harb. Perspect. Biol. *3*, a005272.

Potelle, S., Morelle, W., Dulary, E., Duvet, S., Vicogne, D., Spriet, C., Krzewinski-Recchi, M.A., Morsomme, P., Jaeken, J., Matthijs, G., et al. (2016). Glycosylation abnormalities in Gdt1p/TMEM165 deficient cells result from a defect in Golgi manganese homeostasis. Hum. Mol. Genet. *25*, 1489–1500.

Riblett, A.M., Blomen, V.A., Jae, L.T., Altamura, L.A., Doms, R.W., Brummelkamp, T.R., and Wojcechowskyj, J.A. (2015). A haploid genetic screen identifies heparan sulfate proteoglycans supporting rift valley fever virus infection. J. Virol. *90*, 1414–1423.

Sanjana, N.E., Shalem, O., and Zhang, F. (2014). Improved vectors and genome-wide libraries for CRISPR screening. Nat. Methods *11*, 783–784.

Schimmöller, F., Díaz, E., Mühlbauer, B., and Pfeffer, S.R. (1998). Characterization of a 76 kDa endosomal, multispanning membrane protein that is highly conserved throughout evolution. Gene *216*, 311–318.

Selyunin, A.S., Iles, L.R., Bartholomeusz, G., and Mukhopadhyay, S. (2017). Genome-wide siRNA screen identifies UNC50 as a regulator of Shiga toxin 2 trafficking. J. Cell Biol. *216*, 3249–3262.

Shalem, O., Sanjana, N.E., Hartenian, E., Shi, X., Scott, D.A., Mikkelson, T., Heckl, D., Ebert, B.L., Root, D.E., Doench, J.G., and Zhang, F. (2014). Genome-scale CRISPR-Cas9 knockout screening in human cells. Science *343*, 84–87.

Shaner, N.C., Lambert, G.G., Chammas, A., Ni, Y., Cranfill, P.J., Baird, M.A., Sell, B.R., Allen, J.R., Day, R.N., Israelsson, M., et al. (2013). A bright monomeric green fluorescent protein derived from *Branchiostoma lanceolatum*. Nat. Methods *10*, 407–409.

Stefanovic, S., and Hegde, R.S. (2007). Identification of a targeting factor for posttranslational membrane protein insertion into the ER. Cell *128*, 1147–1159.

Tanaka, A., Tumkosit, U., Nakamura, S., Motooka, D., Kishishita, N., Priengprom, T., Sa-Ngasang, A., Kinoshita, T., Takeda, N., and Maeda, Y. (2017). Genome-wide screening uncovers the significance of N-sulfation of heparan sulfate as a host cell factor for chikungunya virus infection. J. Virol. *91*, e00432–17.

Tian, S., Muneeruddin, K., Choi, M.Y., Tao, L., Bhuiyan, R.H., Ohmi, Y., Furukawa, K., Furukawa, K., Boland, S., Shaffer, S.A., et al. (2018). Genome-wide CRISPR screens for Shiga toxins and ricin reveal Golgi proteins critical for glycosylation. PLoS Biol. *16*, e20006951.

Wang, T., Wei, J.J., Sabatini, D.M., and Lander, E.S. (2014). Genetic screens in human cells using the CRISPR-Cas9 system. Science *343*, 80–84.

Woo, C.H., Gao, C., Yu, P., Tu, L., Meng, Z., Banfield, D.K., Yao, X., and Jiang, L. (2015). Conserved function of the lysine-based KXD/E motif in Golgi retention for endomembrane proteins among different organisms. Mol. Biol. Cell *26*, 4280–4293.

Yamaji, T., and Hanada, K. (2015). Sphingolipid metabolism and interorganellar transport: localization of sphingolipid enzymes and lipid transfer proteins. Traffic *16*, 101–122.

Yamaji, T., Nishikawa, K., and Hanada, K. (2010). Transmembrane BAX inhibitor motif containing (TMBIM) family proteins perturbs a trans-Golgi network enzyme, Gb3 synthase, and reduces Gb3 biosynthesis. J. Biol. Chem. *285*, 35505–35518.

Yamashita, T., Wada, R., Sasaki, T., Deng, C., Bierfreund, U., Sandhoff, K., and Proia, R.L. (1999). A vital role for glycosphingolipid synthesis during development and differentiation. Proc. Natl. Acad. Sci. U S A *96*, 9142–9147.

Yang, J.S., Valente, C., Polishchuk, R.S., Turacchio, G., Layre, E., Moody, D.B., Leslie, C.C., Gelb, M.H., Brown, W.J., Corda, D., et al. (2011). COPI acts in both vesicular and tubular transport. Nat. Cell Biol. *13*, 996–1003.

Zeevaert, R., Foulquier, F., Jaeken, J., and Matthijs, G. (2008). Deficiencies in subunits of the Conserved Oligomeric Golgi (COG) complex define a novel group of Congenital Disorders of Glycosylation. Mol. Genet. Metab. *93*, 15–21.

Zolov, S.N., and Lupashin, V.V. (2005). Cog3p depletion blocks vesicle-mediated Golgi retrograde trafficking in HeLa cells. J. Cell Biol. *168*, 747–759.

ISCI, Volume *11*

Supplemental Information

A CRISPR Screen Identifies LAPTM4A and TM9SF Proteins as Glycolipid-Regulating Factors

Toshiyuki Yamaji, Tsuyoshi Sekizuka, Yuriko Tachida, Chisato Sakuma, Kanta Morimoto, Makoto Kuroda, and Kentaro Hanada

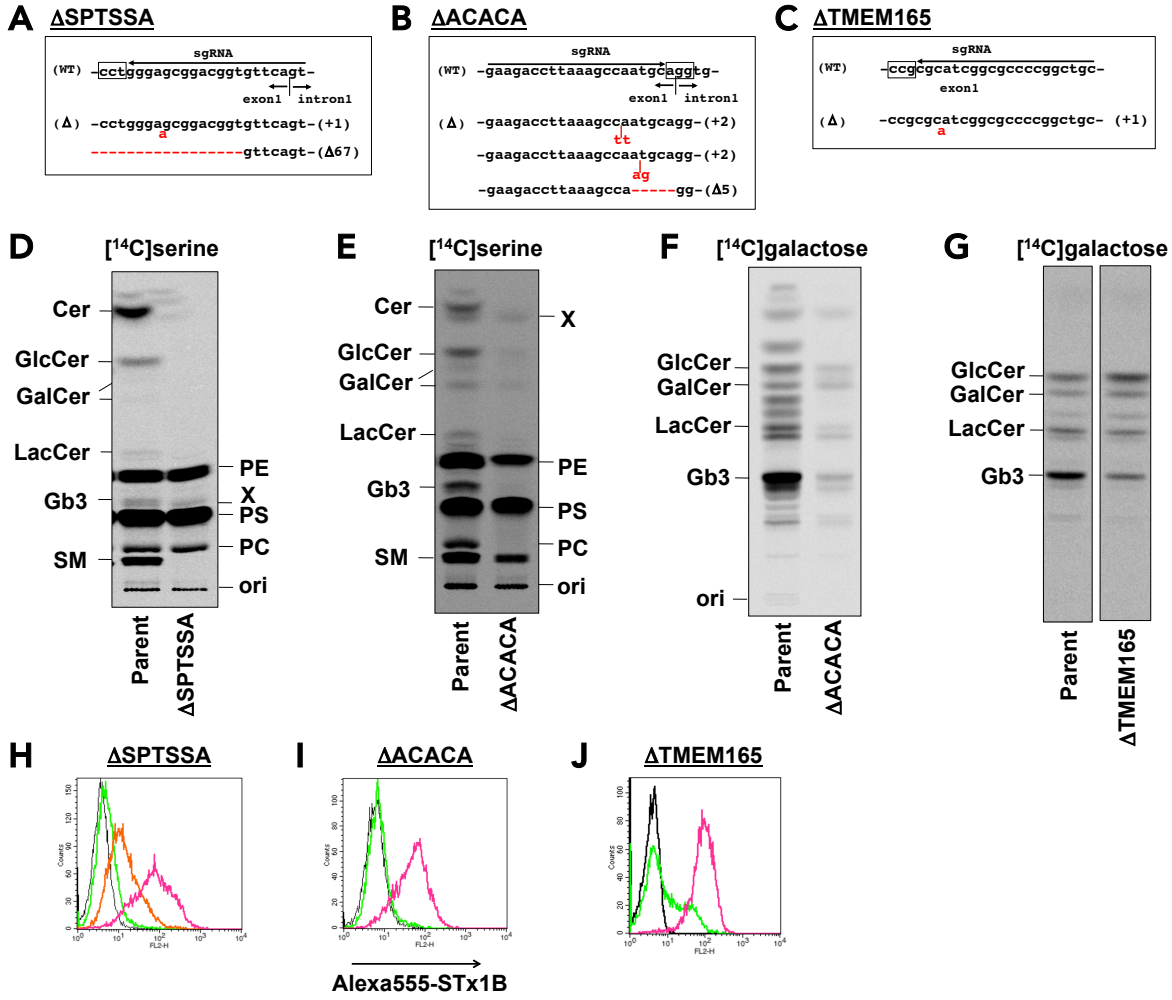

Figure S1. Verification of Gb3 Reduction in Sphingolipid-Related Gene KO Cells, Related to Figure 1.

(A-C) Construction of *SPTSSA*- (A), *ACACA*- (B), and *TMEM165*- (C) KO HeLa cells. Red letters in sequences indicate deletion or insertion mutations, which cause frameshifts shown at the right side of the sequences. Boxes are indicative of protospacer adjacent motif (PAM) sequences.

(D-G) GSL metabolic analysis in sphingolipid-related KO cells. Cells shown in A-C were labeled with [^{14}C]serine (D, E), or [^{14}C]galactose (F, G), and labeled lipids treated with (G) or without (D-F) mild alkali-catalyzed methanolysis were separated on a TLC plate.

(H-J) Surface binding of STx on KO cells. Indicated cells were stained with (yellow-green, orange and magenta lines) or without (black line) Alexa555-STx1B and analyzed by FACS. (H) Yellow-green line indicates staining in KO cells without any other treatment, and the effect of sphingosine addition on STx binding is indicated by the orange line (2μM) and the magenta line (7.5μM). The addition of sphingosine compensates for defective sphingolipid biosynthesis through the salvage pathway. (I) The yellow-green line indicates staining in KO cells without any other treatment, and the effect of palmitate addition on STx binding is indicated by the magenta line (100μM). The addition of palmitate compensates for defective fatty acid biosynthesis. (J) The yellow-green line indicates staining in KO cells without any introduction of cDNA, and magenta line indicates staining in KO cells expressing TMEM165 cDNAs.

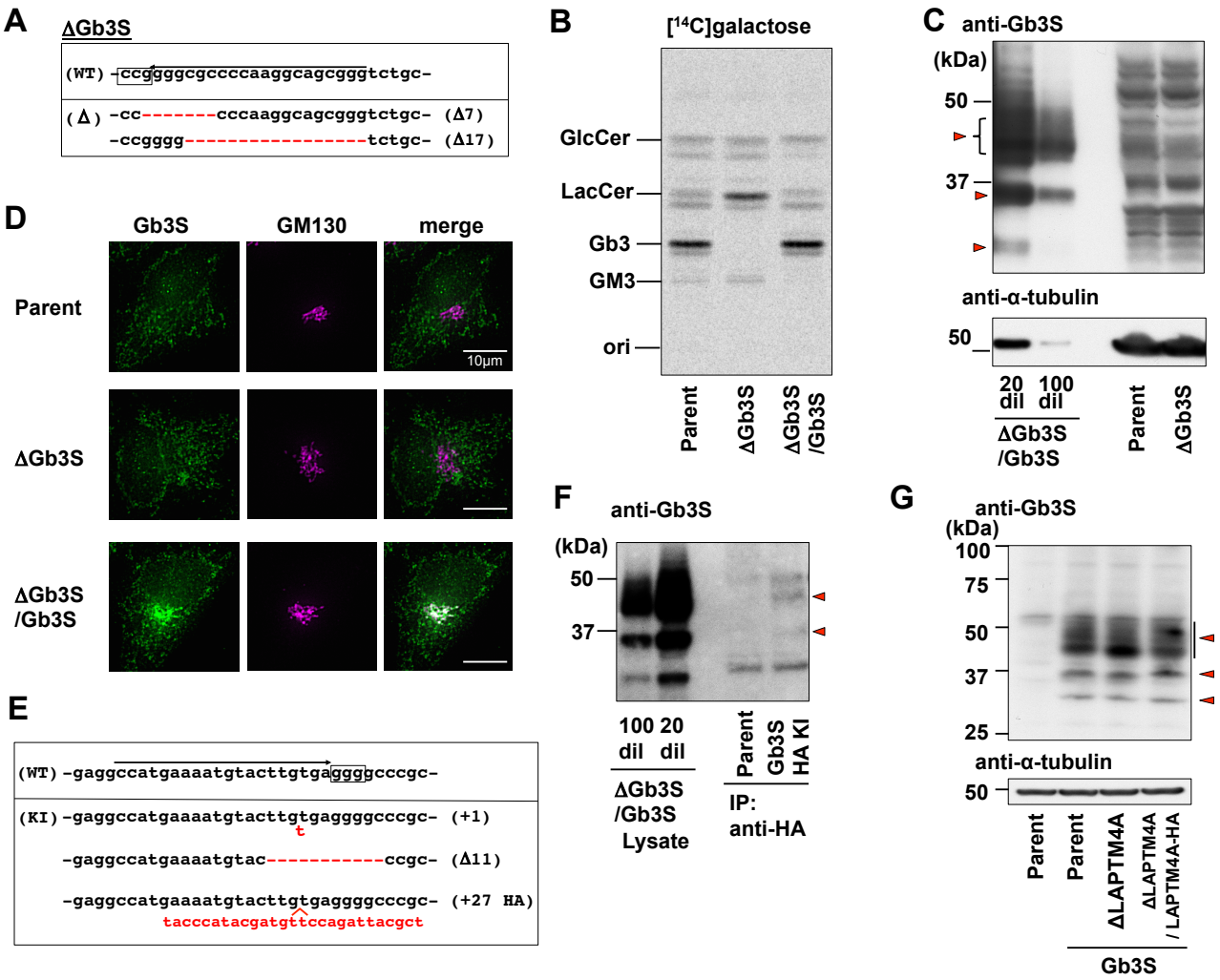

Figure S2. Endogenous Gb3 Synthase Cannot Be Detected Due to Low Expression, Related to Figure 3.

(A) Construction of *Gb3S*-KO HeLa cells. Red letters in sequences indicate deletion mutations, which cause frameshifts shown at the right side of the sequences. Boxes are indicative of PAM sequences.

(B) GSL metabolic analysis in Gb3S-KO cells. Cells were labeled with [^{14}C]galactose, and the labeled lipids were separated on a TLC plate.

(C) Western blot analysis of Gb3S proteins. Parent cells, *Gb3S*-KO cells (ΔGb3S), and Gb3S cDNA-reintroduced cells (ΔGb3S/Gb3S), were analyzed. Lysates of ΔGb3S/Gb3S were loaded at 20- and 100-fold dilutions. Triangles are indicative of Gb3S proteins (complex type, high mannose type, and non-glycosylation type from the top (Yamaji et. al., 2010)). Note that expression level of endogenous Gb3S proteins was lower than that of exogenous Gb3S at 100-fold dilution.

(D) Immunofluorescence analysis of Gb3S proteins. Parent cells, ΔGb3S cells, and ΔGb3S/Gb3Scells were stained with anti-Gb3S antibodies and anti-GM130 (Golgi). Scale bars, 10 μm and 1 μm. Note that endogenous Gb3S was undetected in this condition.

(E) Construction of *Gb3S*-HA knock-in HeLa cells (Gb3S-HA KI). The HA tag sequence was inserted to one of three *Gb3S* gene alleles at the C-terminal side.

(F) Western blot analysis of Gb3S-HA proteins. Lysates of parent cells and Gb3S-HA KI cells were immunoprecipitated with anti-HA agarose. The immunoprecipitates and lysate of ΔGb3S/Gb3S were loaded. Triangles are indicative of Gb3S-HA proteins.

(G) Levels of exogenously expressed Gb3S in parent cells, ΔLAPTM4A cells, and ΔLAPTM4A/LAPTM4A cells. Retrovirally expressed Gb3S proteins in the indicated cells were analyzed by western blotting using anti-Gb3 synthase antibodies. Triangles are indicative of Gb3S proteins.

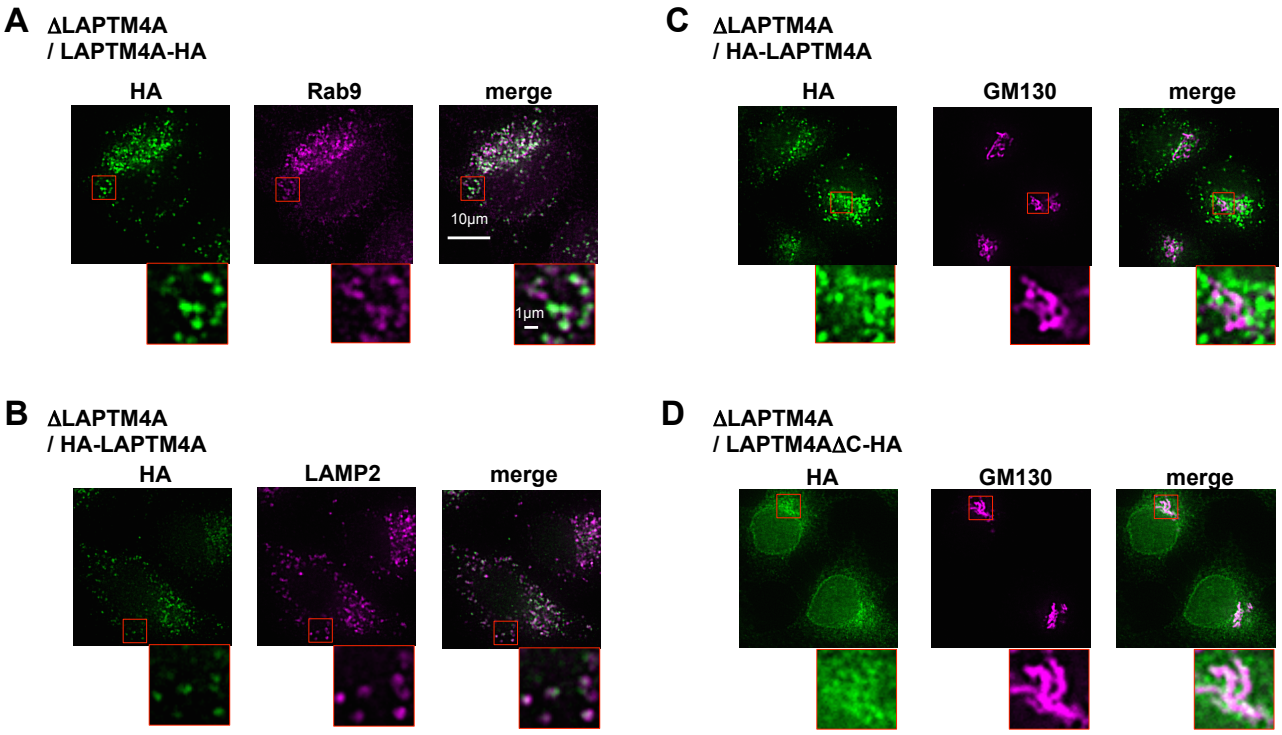

Figure S3. Intracellular Localization of LAPTM4A-HA, HA-LAPTM4A, and LAPTM4AΔC-HA, Related to Figure 4.

ΔLAPTM4A/LAPTM4A-HA, ΔLAPTM4A/HA-LAPTM4A and ΔLAPTM4A/LAPTM4AΔC-HA cells were stained with anti-HA antibodies and the indicated marker antibodies (anti-LAMP2 (lysosome and late endosome), anti-Rab9 (late endosome), anti-GM130 (Golgi)). Scale bars, 10 μm and 1 μm.

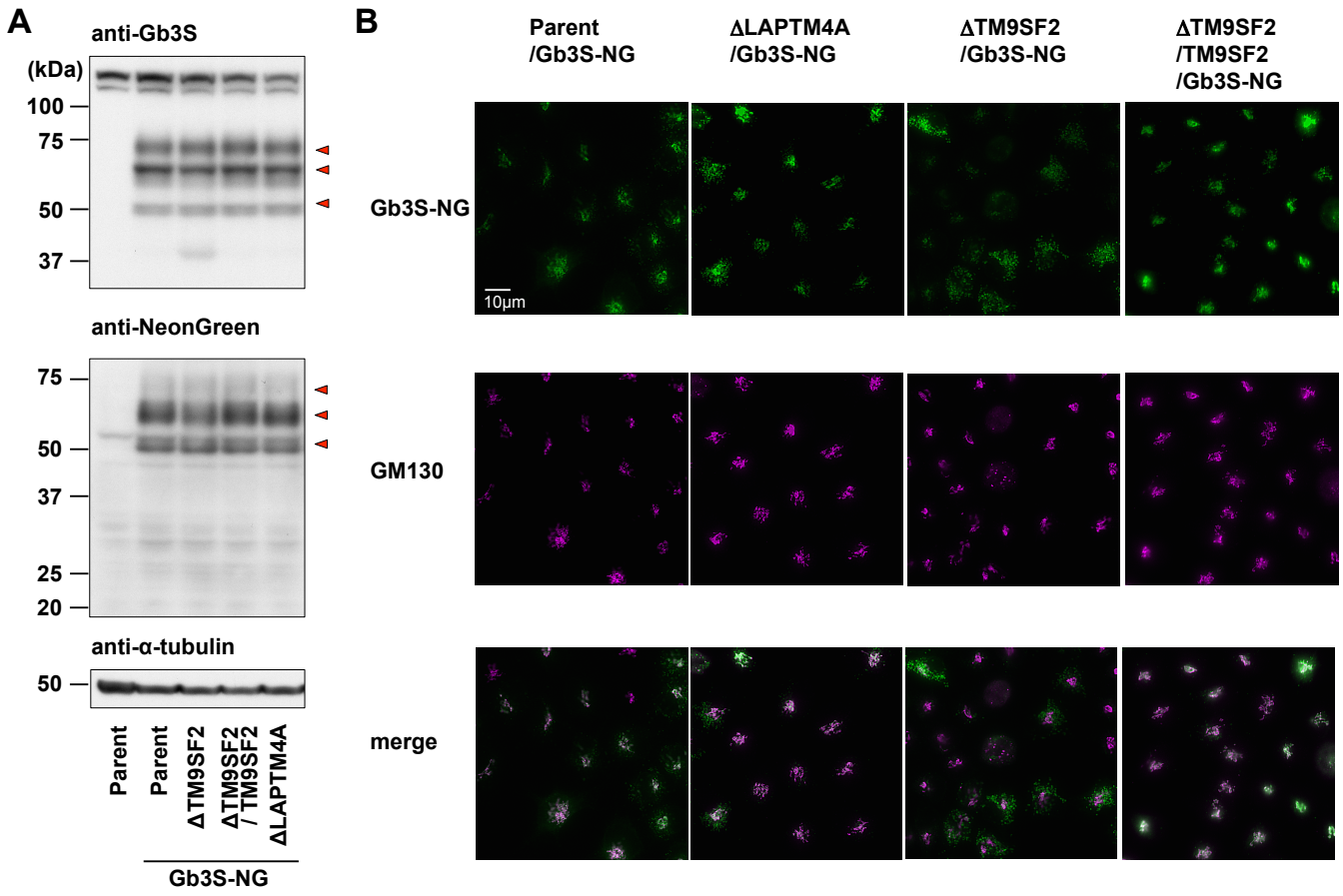

Figure S4. Expression of Gb3S-moxNeonGreen, Related to Figure 5 and 7.

(A) Western blot analysis of Gb3S-moxNeonGreen (NG) proteins. Gb3S-NG was retrovirally expressed in parent cells, *TM9SF2*-KO cells, TM9SF2-rescued cells, and *LAPTM4A*-KO cells. Expression of Gb3S-NG was examined using anti-Gb3S and anti-NeonGreen. Triangles are indicative of Gb3S-NG proteins.

(B) Intracellular localization of Gb3S-NG. Parent/Gb3S-NG cells, ΔTM9SF2/Gb3S-NG cells, ΔTM9SF2/TM9SF2/Gb3S-NG cells, and ΔLAPTM4A/Gb3S-NG cells were stained with anti-GM130 antibodies. Scale bars, 10 μm.

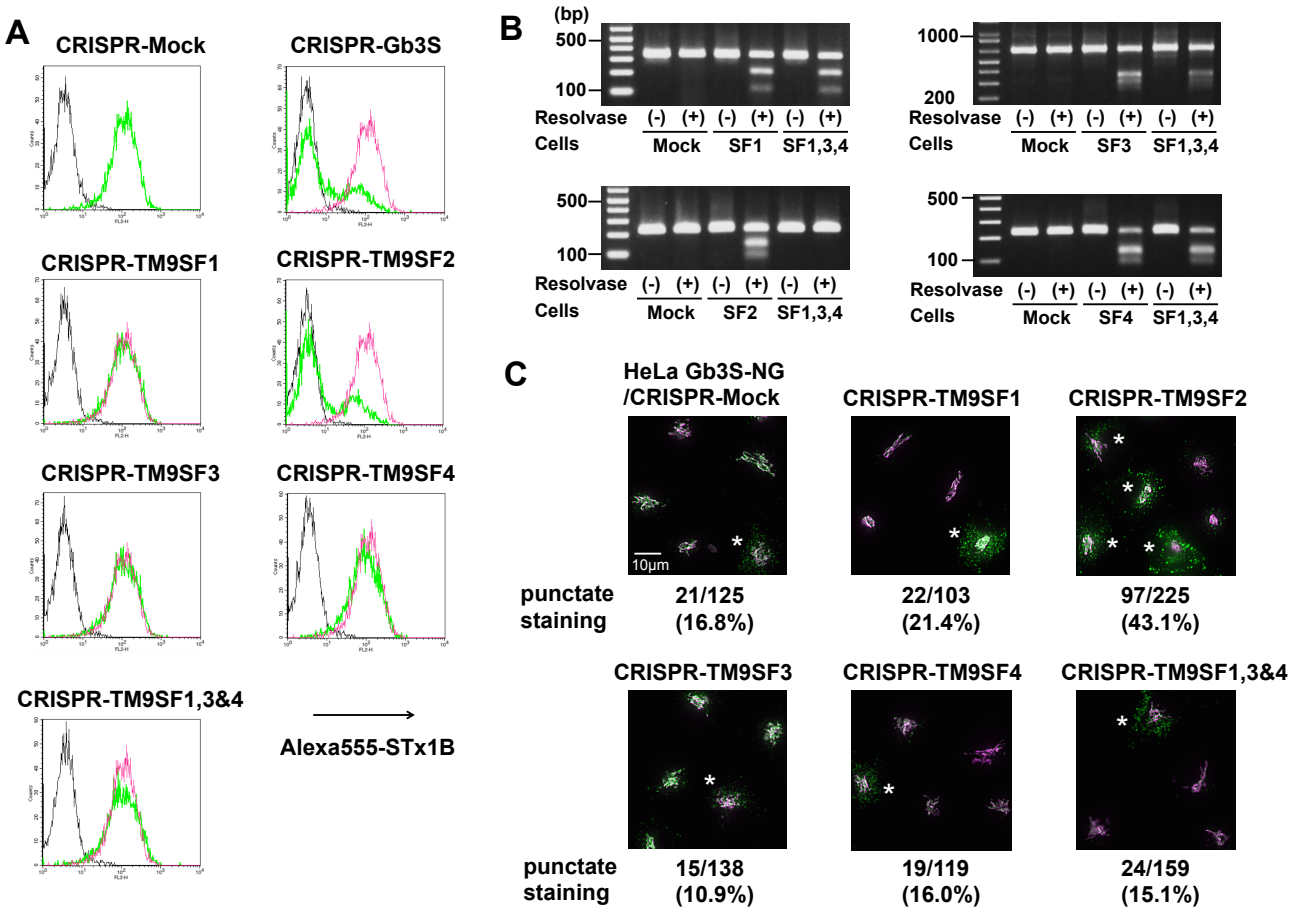

Figure S5. Disruption of Other TM9SF family Genes does not Affect Gb3 Metabolism, Related to Figure 6.

(A) Surface binding of STx on cells treated with sgRNAs targeting TM9SF family members. HeLa cells were treated with sgRNAs targeting to TM9SF1–4, a mixture of TM9SF1, 3, & 4 and A4GalT as well as mock and stained with (yellow-green and magenta lines) or without (black line) Alexa555-STx1B and analyzed using FACS. Magenta lines indicate staining in mock-treated cells as the upper left histogram.

(B) Mutation analysis of sgRNA-treated cells. Genomic PCR fragments containing mutation sites from the cells described in (A) were digested with Resolvase. Cleavage of fragments reflects the degree of mutations.

(C) Intracellular localization of Gb3S-NG in sgRNA-treated cells. Parent/Gb3S#IB1 cells were treated with sgRNAs targeting to TM9SF1–4 and a mixture of TM9SF1, 3, & 4 as well as mock vector. Asterisks are indicative of dispersed punctate staining of Gb3S-NG. Cells were stained with anti-GM130 antibodies. Scale bars, 10 μm.

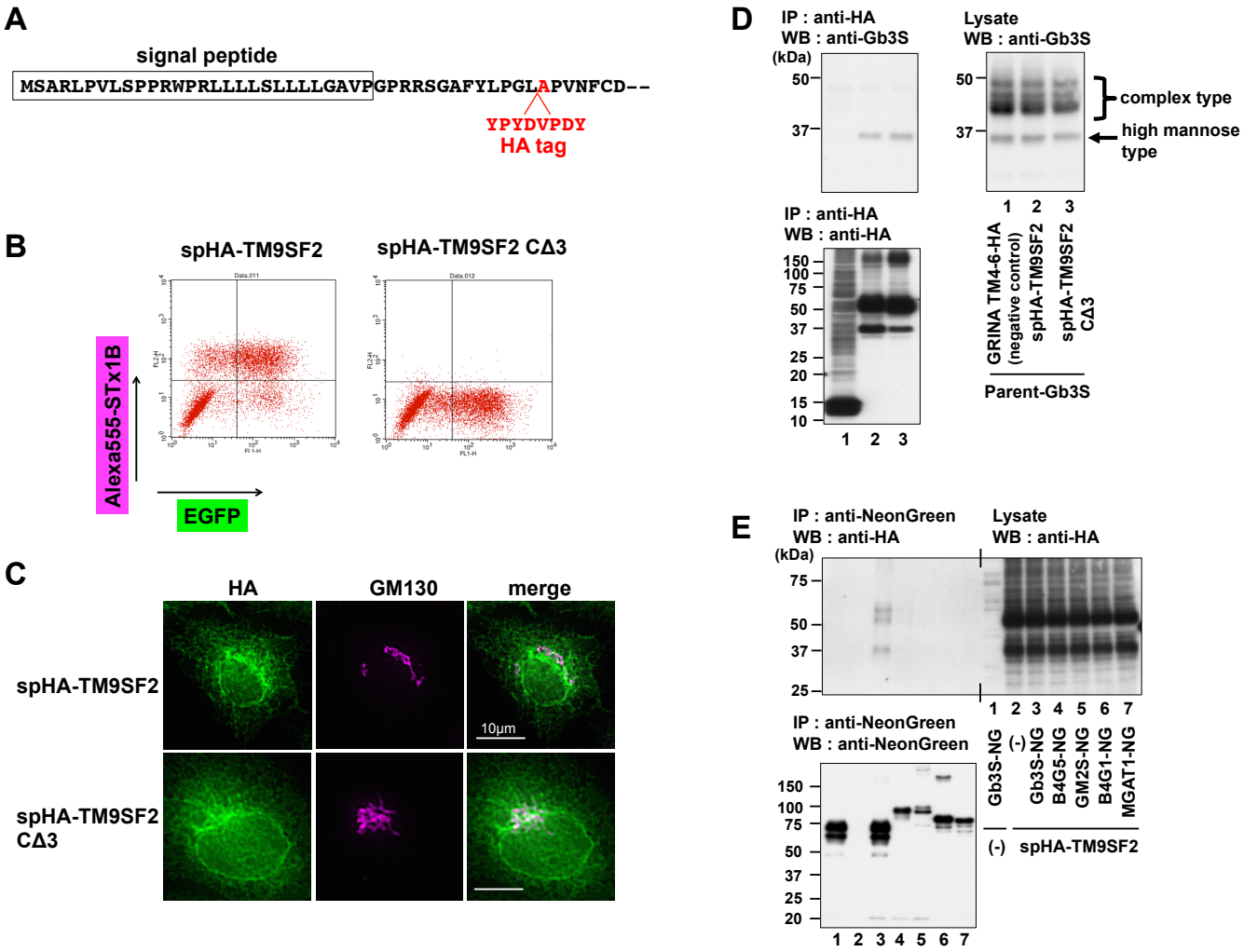

Figure S6. TM9SF2 Interacts with Gb3 Synthase, Related to Figure 6.

(A) Construction of HA-tagged TM9SF2 (spHA-TM9SF2). The HA tag sequence was inserted following the signal peptide.

(B) Effects of spHA-TM9SF2 proteins on STx binding. cDNAs coding spHA-TM9SF2 and spHA-TM9SF2 CΔ3 proteins were transiently transfected with EGFP cDNA into *TM9SF2*-KO cells, and cells were stained with Alexa555-STx1B and analyzed by FACS.

(C) Intracellular localization of spHA-TM9SF2. spHA-TM9SF2 and spHA-TM9SF2 CΔ3 plasmid were transiently transfected to HeLa cells (parent cells), and cells were stained with anti-HA and anti-GM130 antibodies. Scale bars, 10 μm.

(D) Co-immunoprecipitation of Gb3 synthase with spHA-TM9SF2. Plasmids encoding GRINA TM4-6-HA, spHA-TM9SF2, and spHA-TM9SF2 CΔ3 were transiently transfected into parent cells. Cells were lysed and immunoprecipitated with anti-HA agarose. Immunoprecipitates (IP) and lysates were subjected to SDS-PAGE and Western blot (WB) with the indicated antibodies.

(E) Co-immunoprecipitation of spHA-TM9SF2 with various glycosyltransferases. spHA-TM9SF2 plasmid was transfected into parent cells expressing Gb3S-NG, B4GalT5 (B4G5)-NG, GM2 synthase (GM2S)-NG, B4GalT1 (B4G1)-NG, and MGAT1-NG. Cells were lysed and immunoprecipitated with anti-NeonGreen magnetic beads. Immunoprecipitates (IP) and lysates were subjected to SDS-PAGE and Western blot (WB) with the indicated antibodies.

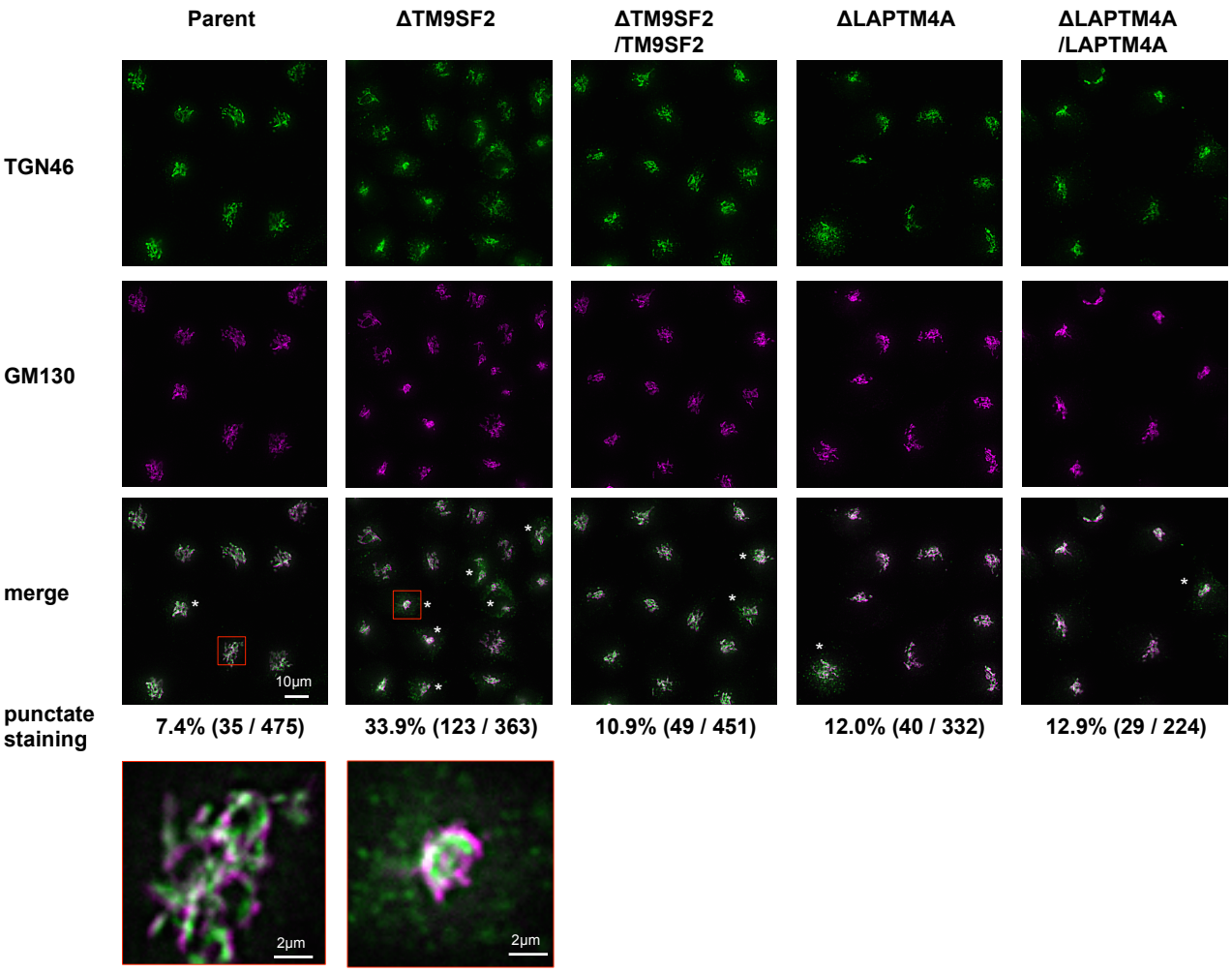

Figure S7. Disruption of TM9SF2 Perturbs Localization of TGN46, Related to Figure 7.

Parent cells, ΔTM9SF2 cells, ΔTM9SF2/TM9SF2 cells, ΔLAPTM4A cells, and ΔLAPTM4A/LAPTM4A cells were stained with anti-GM130 (cis/medial Golgi) and anti-TGN46 (TGN) antibodies. Asterisks are indicative of dispersed punctate TGN46 staining. Scale bars, 10 μm and 2 μm.

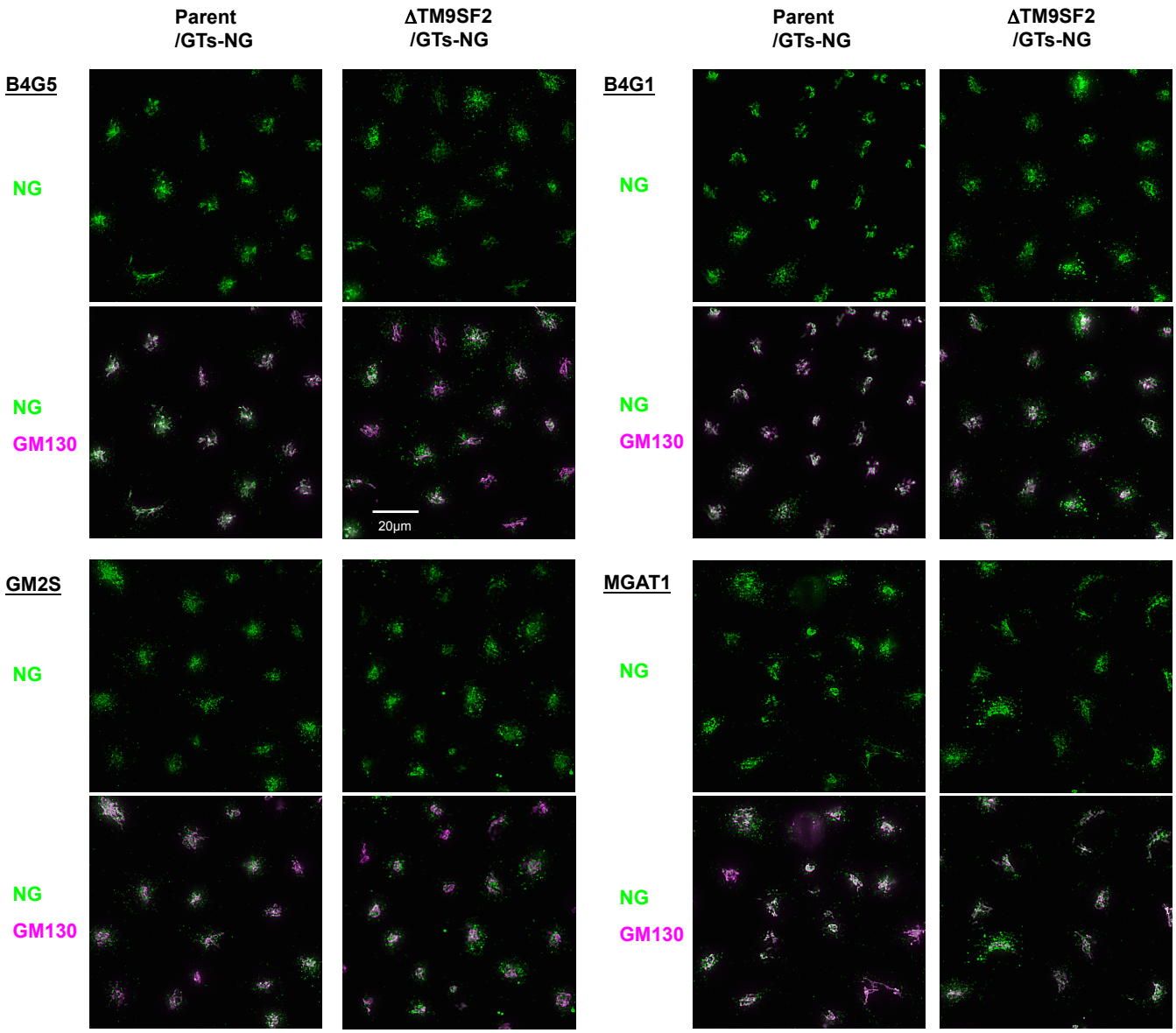

Figure S8. Intracellular Distribution of Glycosyltransferases in ΔTM9SF2 Cells, Related to Figure 7. Parent cells and ΔTM9SF2 cells, expressing Gb3S-NG, B4GalT5 (B4G5)-NG, GM2 synthase (GM2S)-NG, B4GalT1 (B4G1)-NG, and MGAT1-NG, were stained with anti-GM130. Scale bars, 20 μm.

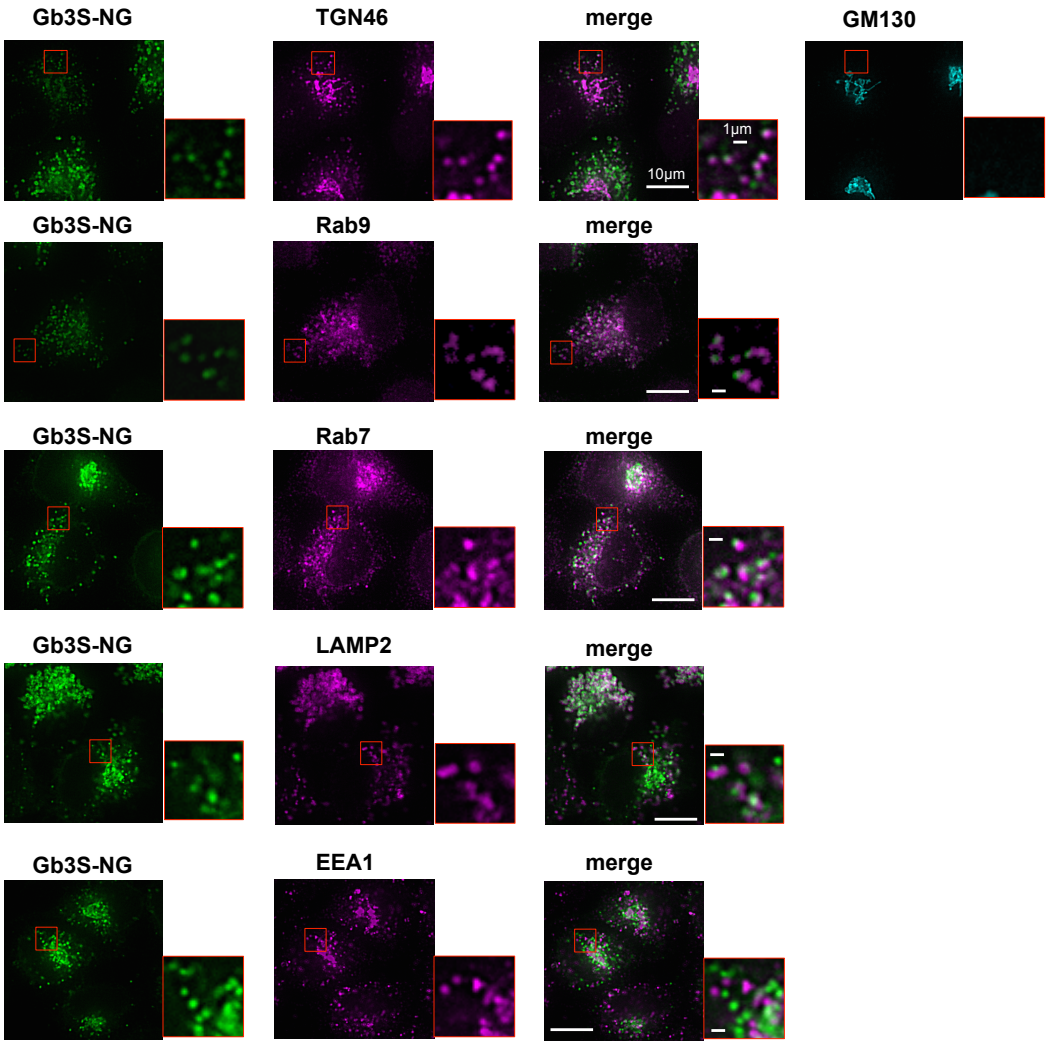

Figure S9. Colocalization of Dispersed Punctate Structures with TGN46, Related to Figure 7. ΔTM9SF2/Gb3S-NG cells were stained with the indicated antibodies (anti-GM130 (cis/medial-Golgi), anti-TGN46 (TGN), anti-Rab9 (late endosome), anti-Rab7 (late endosome), anti-LAMP2 (lysosome and late endosome), and anti-EEA1 (early endosome)). Scale bars, 10 μm and 1 μm.

TRANSPARENT METHODS

Cell Culture, Antibodies, and Reagents

The HeLa-mCAT#8 clone, which expresses mouse cationic amino acid transporter 1 (which serves as the mouse ecotropic retroviral receptor) (Yamaji et al., 2010), and its KO mutants and transfectants were maintained in Dulbecco's modified Eagle's medium (DMEM) containing 10% heat-inactivated fetal bovine serum (FBS) and 4.5 g/L glucose. 293FT cells (ThermoFisher, Rockford, USA) used for lentivirus production were maintained in DMEM containing 10% FBS with non-essential amino acids and sodium pyruvate. Plat-E cells (Morita S et al., 2000) for retrovirus production were maintained in DMEM containing 10% FBS with 1 μg/ml puromycin and 10 μg/ml blasticidin. Sphingolipid-remodeled cells including Gb3 synthase knockdown cells (shGb3S), UGCG KO cells, B4GalT KO cells, and ST3Gal5-overexpressing cells were constructed and described previously (Yamaji et al., 2010, Yamaji et al, 2014).

Purchased antibodies (Abs) were as follows: rabbit anti-LAPTM4A Abs (N-term) (Abgent, SanDiego, USA), rabbit anti-TM9SF2 Abs (ThermoFisher), rabbit anti-Gb3 synthase Abs and rat anti-HA IgG (Sigma-Aldrich, St. Louis, MO), mouse anti-GM130 IgG and mouse anti-EEA1 IgG (BD Transduction Laboratories, San Diego, CA), sheep anti-TGN46 Abs (Serotech, Kidlington, UK), mouse anti-Rab9 IgG (Merck Millipore, Darmstadt, Germany), rabbit anti-Rab7 Abs and rabbit anti-mNeonGreen Abs (Cell Signaling, Danvers, USA), mouse anti-LAMP2 IgG (Santa Cruz Biotechnology, Dallas, USA), mouse anti-mNeonGreen IgG (Chromotek, Planegg-Martinsried, Germany). Chicken anti-VAP-A Abs were raised against the recombinant cytosolic domain of human VAP-A and affinity-purified as described previously (Yamaji et al., 2010). Alexa-conjugated secondary antibodies were purchased from ThermoFisher, except Alexa-594 donkey anti-sheep $F(ab')_2$ fragment, which was purchased from Jackson ImmunoResearch (West Grove, USA).

3-(4,5-Dimethylthiazoyl-2-yl)-2,5-diphenyltetrazolium bromide (MTT) and puromycin were purchased from Sigma-Aldrich. Thin-layer chromatograpy (TLC), high-performance thin-layer chromatography (HPTLC) plates (Silica Gel 60) and Uridine 5' diphosphate galactose (UDP-Gal) were purchased from Merck (Darmstadt, Germany). D-[1-^{14}C]Galactose (56 mCi/mmol) was purchased from GE Healthcare (Buckinghamshire, UK). UDP-[6-^{3}H]Gal was purchased from American Radiolabeled Chemicals (St. Louis, USA). L-[U-^{14}C]Serine (174 mCi/mmol) was purchased from Moravek (Brea, USA). Geneticin was purchased from Nacalai Tesque (Kyoto, Japan). Blasticidin-S was purchased from Kaken Pharmaceutical (Tokyo, Japan). Lipofectamine LTX reagent was purchased from

Thermo Fisher. Polyethylenimine Max (PEI-Max) was purchased from Polysciences Inc (Warrington, USA). Shiga toxin 1 (STx1) derived from *E. coli* O157:H7 was a kind gift from Dr. Kiyotaka Nishikawa (Doshisya University, Kyoto, Japan) (Watanabe et al., 2004). Preparation of fluorescent STx1 B subunit (Alexa555-STx1B) was conducted as described previously (Yamaji et al., 2010). The human Genome-scale CRISPR Knock-Out (GeCKO) v2.0 library in the lentiGuide-Puro plasmid (65386 single-guide RNAs (sgRNAs) in library A and 58031 sgRNAs in library B) and the lentiCAS9-Blast plasmid (two vector lentiviral GeCKO system) were obtained from Addgene (Sanjana et al., 2014). Primers used in this study are described below.

Isolation of Cas9-expressing HeLa cell clone for CRISPR screen

293FT cells were transfected with a lentiCAS9-Blast plasmid and ViraPower packaging plasmids (Thermo Fisher) to produce lentivirus for CAS9 expression (CAS9-lentivirus). Subsequently, HeLa mCAT#8 cells were infected with the CAS9-lentivirus, and the CAS9-expresing cells were grown in the presence of 7.5 μg/ml blasticidin. The clone with the highest genome-editing efficiency was selected as the parent cell clone (HeLa CAS9#W7) for the CRISPR screen.

Production of lentiviral CRISPR libraries

For amplification of the GeCKO v2.0 library plasmids, 300 ng of the library A and B plasmids were separately transformed into ElectroTen-Blue Electroporation-Competent cells (Agilent, Santa Clara, USA) using a Gene Pulser Xcell (BIO-RAD, Hercules, USA), and the plasmids were purified from approximately 5–10 × 10^7 colonies of transformed *E.coli* using an Endotoxin-free Plasmid DNA Extraction Maxi Kit (Favorgen, Ping-Tung, Taiwan). Two independent lentiviral pools (#1 and #2) of the library were produced. Briefly, approximately 1 × 10^8 (#1) and 7 × 10^7 (#2) 293FT cells were transfected with 48 μg (#1) and 30 μg (#2) of the library plasmids and ViraPower packaging plasmids (Thermo Fisher) using PEI Max (#1) and Lipofectamine LTX with Plus reagent (#2). After 24 hours, media was changed and the cells were cultured for 24 additional hours. Subsequently, culture media containing secreted lentiviruses was filtered using a 0.45 μm bottle top filter and frozen as lentiviral pools (A-1, A-2, B-1, B-2).

Preparation of sgRNA-expressing cell libraries

HeLa CAS9#W7 cells (2 × 10^7 cells) were infected with each lentivirus pool at a low MOI (about 0.2). Twenty-four hours after transduction, cells were selected with 1 μg/ml puromycin for three days and cultured for an additional five days to prepare sgRNA-expressing HeLa cell libraries.

CRISPR screen for STx1 treatment

2.4×10^7 sgRNA-expressing cells from each cell library (A-1, A-2, B-1, B-2) were plated 24 hours prior to treatment with 50 pg/ml STx1. Three days after the STx1 treatment, cells were cultured in the absence of Stx1 for 8 days. Surviving cells were then re-plated and treated with 50 pg/ml STx1 again. Two days after treatment, cells were trypsinized and frozen as cell pellets. For untreated controls, 1.2×10^7 sgRNA-expressing cells in each cell library were cultured for the same period as STx1-treated cells with several passages, such that a minimum of 1.2×10^7 cells was present in each passage.

Genomic DNA sequencing

Analysis of genome-integrated sgRNAs was based on new generation sequencing using MiSeq (Illumina, San Diego, USA). Genomic DNA from frozen cells was purified using the conventional phenol-chloroform method. Briefly, cell pellets were re-suspended in 5ml QIAGEN Buffer P1 with 0.5% SDS, and were sonicated to shear DNA. Subsequently, a phenol/chloroform extraction, a chloroform extraction, and DNA precipitation with isopropanol were performed. Amplification of the genome-integrated sgRNA sequences by PCR was performed as follows, based on a previous report (Shalem et al., 2014). For the first PCR, 100 μg genomic DNA from untreated cells or more than one third of the total amount of isolated genomic DNA from STx1-treated cells were used as PCR templates. For each sample (A-1, A-2, B-1, B-2), nine separate 100 μl reactions were performed using PrimeStar GXL DNA polymerase (Takara, Otsu, Japan) and the following primers (9 forward primers and 1 reverse primer):

(Fw) 1stY1R1s0-8: CTACACGACGCTCTTCCGATCT (0-8 bp random sequence for increasing library complexity) TCTTGTGGAAAGGACGAAACACCG

(Rv) 1stY2as: GCCACTTTTTCAAGTTGATAACGGACTAG

Amplification was carried out with 20 cycles. One (1) μl from these nine separate first PCR products was respectively used as a template for the second PCR. For each sample, nine separate 20 μl PCR reactions were performed using the following primers:

(Fw) 2nd P5R1s: AATGATACGGCGACCACCGAGATCTACA**CTCTTTCCCTACACGACGCTC TTCCGATCT**

(Rv) 2nd P7Y2as: CAAGCAGAAGACGGCATACGAGAT (CC (A-1), or TT (A-2), or AA (B-1), or GG (B-2) as barcodes for multiplexing of different samples) GCCACTTTTTCAAGTTGATAACGGACTAG

Underlines indicate Illumina adaptor sequences (P5 and P7 respectively), with bold letters indicating the sequence

primer site for MiSeq sequence analysis. Amplification was carried out with 10 cycles. The resulting nine amplicons in each sample were mixed and gel extracted using SYBR Gold (ThermoFisher). The extracted DNA was then quantified using a Quantus fluorometer (Promega, Madison, USA) as well as running an agarose gel with 100 bp quantifiable DNA Ladder (NEB, Ipswich, USA), and equal amounts of each sample (A-1, A-2, B-1, B-2) were mixed. The DNA concentration of the mixture was adjusted for sequencing analysis. PhiX Control Kit v3 (Illumina) was added to the sample at approximately 20% concentration. MiSeq Reagent Kit v3 (Illumina) was used for MiSeq sequencing.

Data processing and analysis

To perform demultiplexing of fastq sequence data, total raw read sequences were divided into each sample with barcode sequences of "AA", "CC", "GG" and "TT" using an in-house program. The adapter sequences were removed using a skewer program (version 0.1.126) (Jiang et al., 2014) with the following parameters: minimum read length = 10 mer, maximum read length = 30 mer, lowest mean quality value = 19 sanger quality score. To extract high-quality sgRNA sequences, sequences with a Phread quality score less than 20 were excluded using the "split_libraries_fastq.py" (version 1.9.1) function of the QIIME program (Caporaso et al., 2010). The numbers of the sgRNA sequences were calculated with "sort" and "uniq" of the unix command program, followed by normalization with the following formula; normalized reads per sgRNA = reads per sgRNA / total reads for all sgRNAs in sample x 10^7 (Data S1). Fold enrichment was calculated using the following formula: Fold enrichment = normalized reads in STx-treated sample / normalized reads in untreated sample. When the normalized reads in the untreated sample was 0, fold enrichment was calculated by setting 0 to 1. First, identification of essential genes, which were closely related to STx1 interaction, was performed using the MAGeCK program (version 0.5.7) (Li et al., 2014) to analyze normalized sgRNA count data (Data S3). In this program, 640 genes contained at least one significantly different sgRNA. For stricter selection of hit sgRNAs, the sgRNAs representing more than 1-fold enrichment in both independent cell libraries (A-1 and A-2, or B-1 and B-2) were selected as STx resistance sgRNA candidates (Data S2), and fold enrichment of these candidates were graphed in Figure 1A. Note that the selected sgRNAs were all statistically significantly enriched, which was demonstrated using the MAGeCK program (Data S1 and S2).

Synthesis of CRISPR plasmids

For selection with puromycin to remove untransfected cells in genome-editing, the pSELECT-CRISPR-CAS9 plasmid (Ogawa et al.,2018) was used. The plasmid was cleaved with BsmBI, and a 20-mer guide sequence was

ligated into the site. The sequences of the 20-mer guide sequence were confirmed using an ABI3100 sequencer. The sgRNA sequences used in this study were described below.

Construction of CRISPR KO cell lines

On day 0, HeLa-mCAT8 cells (1.5×10^5 cells/well in 12-well plates) were cultured overnight. On day 1, a CRISPR plasmid was mixed with X-tremeGENE HP (Roche Diagnostics) (in 12-well plates, 1 μg of plasmid and 2 μl X-tremeGENE HP were mixed in 100 ml Opti-MEM), and the mixture was then added to the cells. On day 2, the cells were transferred to 6-well plates and cultured at 37°C with puromycin at 5 μg/ml, which is higher than the usual concentration, in order to concentrate cells with higher sgRNA expression. This step excludes the untransfected cells. On day 5, culture medium was changed to puromycin-free medium, and the cells were subcultured for 3 days. CRISPR-treated HeLa cells were used for STx treatment, and the cell viability assay was conducted as described below (Figure 1B), harvested for indel analysis, or diluted to isolate gene-disrupted clones. To construct HA-tagged knock-in cells by homologous recombination using the CRISPR/CAS system, single-stranded oligonucleotides of C-terminus of Gb3S with HA-tag were transfected together with a CRISPR plasmid targeting Gb3 synthase. The sequence of the single-stranded oligonucleotides is described below.

Indel analysis

Indel analysis was performed as previously described (Yamaji and Hanada, 2014). Briefly, trypsinized cells were heated in TE buffer followed by vortexing to use as a template of genomic PCR. PCR was performed with PrimeSTAR GXL, and blunt-end PCR products were then cloned with a Zero Blunt TOPO PCR Cloning Kit (Invitrogen). After *E.coli* transformation, colony direct PCR or plasmid purification was performed to use as a template for sequence analysis. DNA sequences were determined using an ABI3100 Genetic Analyzer (Applied Biosystems). KO cell clones of *LAPTM4A*, *TM9SF2*, *SPTSSA*, *ACACA*, *TMEM165*, and *A4GalT* (*Gb3S*) were isolated. A resolvase-based mutation assay using the Guide-it Mutation Detection Kit was performed according to the manufacture's instructions (Takara).

RNA isolation, RT-PCR, and real-time PCR

Total RNA was isolated using the TRIzol Reagent per manufacturer's instructions (Thermo Fisher). RT-PCR was performed using the ReverTra Ace qPCR RT Master Mix (ReverTra Ace, Toyobo) per manufacturer's instructions, including a DNase I treatment step. For real-time PCR, the LightCycler 96 system with LightCycler-FastStart DNA

master SYBR Green I kit (Roche) was used according to the manufacturer's protocol (Yamaji et al., 2010).

cDNA cloning and vector construction

Human *TM9SF1-4*, *LAPTM4A*, *LAPTM4B*, *TMEM165*, and *Gb3 synthase* (*Gb3S*) cDNAs were amplified by PCR (template: *TM9SF1* and *TM9SF3* from thyroid cDNA (Thermo Fisher), *TM9SF4* from placenta cDNA, *Gb3S* from brain cDNA, others from HeLa mCAT#8 cDNA). Amplified DNAs were digested with restriction enzymes and inserted into the vectors as described below. moxNeonGreen (C149T) was prepared from mNeonGreen (Allele Biotechnology, San Diego, USA) by PCR-based mutagenesis to prevent non-native disulphide bonds in the lumen of the Golgi (Shaner et al., 2013, Costantini et al., 2015). Gb3S was fused with moxNeonGreen at the C-terminus to prepare Gb3S-moxNeonGreen fusion protein (Gb3S-NG). The sequences of LAPTM4A and LAPTM4B were aligned using EMBL-EBI EMBOSS Water (https://www.ebi.ac.uk/Tools/psa/emboss_water/). spHA-TM9SF2 was constructed by PCR and Gibson assembly (NEB). $pCXN_2$-GRINA TM4-6-HA plasmid (for use as a negative control) was constructed and described previously (Yamaji et. al., 2010).

Preparation of plasmid-based stable transfectants

$pCXN_2$-TM9SF2 plasmids were linearized and transfected into *TM9SF2*-KO cells using X-tremeGENE HP. The cells were then subjected to geneticin selection at a concentration of 800 μg/ml. Colonies were isolated by limiting dilution. A clone expressing TM9SF2 proteins was selected (ΔTM9SF2/TM9SF2).

Retroviral infection and preparation of stable transfectants

Preparation of retroviruses and infection of HeLa-mCAT#8-based cells were performed using the Plat-E system, as described previously (Morita S et al., 2000). When pMXs-IP-based (Gb3S-NG, B4G5-NG, GM2S-NG, B4G1-NG, MGAT1-NG) and pMXs-IB-based (LAPTM4A, its mutants, LAPTM4B, TMEM165, and Gb3S-NG) retroviruses were used, the concentrations of puromycin and blasticidin-S for selection were 2 μg/ml and 7.5 μg/ml, respectively. Established cells were as follows: ΔLAPTM4A/LAPTM4A, ΔLAPTM4A/LAPTM4A-HA, ΔLAPTM4A/HA-LAPTM4A, ΔLAPTM4A/LAPTM4AΔC-HA ΔLAPTM4A/LAPTM4B-HA, ΔTMEM165/TMEM165, Parent/Gb3S-NG, ΔLAPTM4A/Gb3S-NG, ΔLAPTM4A/LAPTM4A-HA/Gb3S-NG, ΔLAPTM4A/HA-LAPTM4A/Gb3S-NG, ΔLAPTM4A/LAPTM4AΔC-HA/Gb3S-NG, ΔTM9SF2/Gb3S-NG, ΔTM9SF2/TM9SF2/Gb3S-NG, Parent/Gb3S, ΔLAPTM4A/Gb3S, ΔLAPTM4A/LAPTM4A-HA/Gb3S, ΔLAPTM4A/HA-LAPTM4A/Gb3S, and ΔLAPTM4A/LAPTM4AΔC-HA/Gb3S. Gb3S-NG-expressing cells were

further cloned, and representative clones, including Parent/Gb3S-NG#1, #2, Parent/ Gb3S-NG#IB1, ΔTM9SF2/Gb3S-NG#1, #2, and ΔTM9SF2/TM9SF2/Gb3S-NG#1, were used. Mean fluorescence intensities are indicated in the images. HeLa shGb3S cells were constructed and described previously (Yamaji et al., 2010).

Immunofluorescence microscopy

Immunostaining was performed as described previously (Kawano et al., 2006), and specimens were visualized with a wide-field fluorescence microscope, BZ-X700 (Keyence, Osaka, Japan) equipped with a Plan Apo VC 60x1.20 WI (water immersion) objective. Haze reduction function (condition 2), which applies a no-neighbor deconvolution algorithm to the captured image, was used to eliminate fluorescence blurring caused by scattered light and capture clear images with high contrast.

Lysate preparation and Western blot analysis

Two methods were used to prepare lysates as follows. Method 1: Cells were sonicated in sonication buffer (10 mM Hepes/NaOH (pH7.4) 1 mM EDTA, 0.25 M sucrose, protease inhibitor cocktail) and subsequently mixed with Laemmli sodium dodecyl sulfate (SDS) sample buffer. This method was used for the detection of Gb3 synthase. Method 2: Cells were sonicated as in Method 1. For the detection of LAPTM4A, the lysates were ultracentrifuged at 100,000g for 1 hr at 4°C to isolate membrane fractions, followed by suspension in sonication buffer. Then, lysates were mixed with 4 volumes of urea-containing buffer (50 mM Tris/HCl pH 8.8, 7 M urea, 2 M thiourea, 2% CHAPS, 2% Triton X-100, 33 mM DTT, protease inhibitor cocktail), and incubated for 1 hr at 37°C. Proteins were then alkylated with 100 mM iodoacetoamide to prevent re-oxidation of SH residues. Lithium dodecyl sulfate was added to samples at 2%. This method was used for the detection of TM9SF2 and LAPTM4A, which are multispanning membrane proteins. Protein concentrations were determined using the Pierce BCA protein assay kit using BSA as a standard. Proteins were resolved by SDS-PAGE, transferred to PVDF membranes using the wet transfer method, and probed with specified antibodies. Antigen signals were detected using SuperSignal West Femto Maximum Sensitivity Substrate (ThermoFisher Scientific) or Chemi-Lumi One L (Nacalai, Kyoto, Japan) and exposed to an X-ray film. To detect TM9SF2, urea-containing polyacrylamide gels were used, as the predicted molecular size of TM9SF2 band deviated from the molecular marker (Bio-rad, Hercules, USA) when urea was not included, suggesting urea was required for protein denaturation.

Immunoprecipitation analysis

Cells were lysed with Lysis buffer (50mM Tris/HCl pH8.0, 150mM NaCl, 1mM EDTA, 1% Triton). After

centrifugation, the cell lysate supernatants were incubated with anti-HA agarose beads (Sigma) or mNeonGreen magnetic agarose beads (Chromotek). After washing with Lysis buffer, bound proteins were eluted with SDS sample buffer.

Metabolic labeling of glycolipids and TLC analysis

Metabolic labeling experiments using L-[U-^{14}C]serine and D-[1-^{14}C]galactose including mild alkaline methanolysis were performed as described previously (Yamaji et al., 2016). Cells (3×10^5/well in a 6-well plate) were cultured overnight at 37°C, and cells were then incubated with 22.2 kBq of L-[U-^{14}C]serine or 7.4 kBq of D-[1-^{14}C]galactose in Opti-MEM with 1% Neutridoma-SP (Roche) for 16 h. Cells were lysed with 0.1% sodium dodecyl sulfate (SDS), and lysates containing the same amount of protein were then used for lipid extraction following the method of Bligh and Dyer (Bligh and Dyer 1959). For alkali-methanolysis to remove glycerolipids, dried lipids were hydrolyzed with 0.1N KOH in methanol for 1 hr at 40°C. After neutralization with 0.1N HCl, the methanol layer was washed with *n*-hexane twice, and the lipids were extracted using the method of Bligh and Dyer. The lower fractions collected were dried under an N_2 gas stream. Separation of lipids by TLC was performed using two methods as follows. Method 1: A TLC60 plate (20 cm × 20 cm), developing solvent: methyl acetate/n-propanol/chloroform/methanol/0.25% KCl = 50/50/50/20/18 (Yamaji et al., 2014), or Method 2: A HPTLC60 plate (10 cm × 20 cm), developing solvent: chloroform/methanol/0.25% $CaCl_2$ = 65/35/8 (Yamaji et al., 2010). Method 1 was used in Figures 2E, S1D, and S1E, and Method 2 was used in Figures 3B, S1F, and S1G. The radioactive lipids on TLC plates were visualized, and the intensity of each band was quantified using a Typhoon FLA 7000 (GE Healthcare, Buckinghamshire, UK). To compare relative amounts of the lipids, the band intensity of each GSL in the parent cells was considered to be 100%.

Measurement of *in vitro* Gb3 synthase activity

To measure Gb3 synthase activity *in vitro,* 5×10^6 cells/plate in a 15cm plate were cultured overnight at 37°C, and cells were then scraped and sonicated in sonication buffer (10 mM Hepes/NaOH (pH7.4), 1 mM EDTA, 15 mM $MnCl_2$, 0.5% Triton X-100, 0.25 M sucrose, protease inhibitor cocktail (Roche)). The lysates were adjusted by total protein concentration, which was used as an enzyme source. Twenty-five micrograms of LacCer (or no lipid) and 300 μg Triton X-100 were dissolved in chloroform, which was removed from the mixture using an N_2 gas stream. Dried lipids were sonicated in 90 μl reaction buffer (20 mM MES/NaOH (pH 6.4), 15 mM $MnCl_2$, 6.25 μM UDP-galactose) and substrates were then incubated with 25 pmol (0.5 μCi) of UDP-[6-^{3}H]galactose and 10 μl of the prepared lysates for 1 hr at 37°C. Lipids in the reaction mixture were extracted using the method of Bligh and Dyer.

Separation of the lipids by TLC was performed through Method 2 described above. Visualization and analysis of the labeled lipids were performed as above. The value of the band intensity with LacCer minus the band intensity without LacCer was regarded as the relative Gb3 synthase activity. To compare relative Gb3 synthase activity, the value in the parent cells was considered to be 100%.

FACS analysis

Non-confluent cells were trypsinized and washed with culture medium and wash buffer (1% BSA) in PBS at 4°C. Cells were incubated with 10 μg/ml Alexa-555 Stx1 B subunits for 45min on ice. After washing with wash buffer once, cells were analyzed using a FACSCalibur (BD Biosciences, Franklin Lakes, USA). To determine the effect of transiently expressed proteins on the expression of STx receptors, TM9SF2 KO cells ($2.5x10^4$ cells/well in a 12-well plate) were co-transfected with 0.5 μg $pCXN_2$ plasmids containing the target genes (TM9SFs and TM9SF2 mutants) and 0.05 μg EGFP-N3 (Clontech, Mountain View, USA). After two days of transfection, cells were subjected to FACS analysis. Spillover of EGFP fluorescence in the FL2 channel, and spillover of Alexa-555 in the FL1 channel were electronically compensated. After gating out debris and cell aggregates by FSC/SSC, the percentage of StxR upper cells in EGFP-positive cells was calculated by (cell number in upper right) / (cell number in upper and lower right) x 100.

STx treatment and cell viability assay

To treat with STx1, cells ($1\text{-}1.5x10^4$ cells/ml in 12-well or 24-well plates) were cultured overnight at 37°C, and then treated with STx1 at the indicated concentrations for three days. An MTT assay was then performed as described previously to assess cell viability (Yamaji et al., 2010).

Statistical analysis

A two-tailed unpaired Student's *t*-test was used for statistical analysis, with $p < 0.05$ considered to be statistically significant. For multiple comparisons, the Student's *t*-test with Bonferroni correction was used, with $p < 0.01$ (0.05 divided by 5) considered to be statistically significant in five comparisons (Figure 2F, 3A, and 3C) and $p < 0.0083$ (0.05 divided by 6) considered to be statistically significant in six comparisons (Figure 2C).

Primers used in this study

Primers for indel analysis

hTM9SF2 5UTRs: CCTTGTAGTCGTCTCCGAGAC

hTM9SF2 Ex1as: TCTTCGTCGCAGAAGTTGACGG

hLAPTM4A 5UTRs: CGTGAAACAGCCGTTTGAGTTTGG

hLAPTM4A Ex1as: ATGTACCAGGTCCCCAGGATG

hSPTSSA 5UTRs: GACAGACTGACGTGTGAGCTG

hSPTSSA Int1as: GGATCTCAAGAGTTCTCGTCTCC

hACACA-Ex9s: GTTCTTATTGCTAACAATGGCATTGCAGC

hACACA-Int9as: CCTACTTAAAGGCTGTGCTGTTCCATG

hTMEM165 5UTRs: TGTTCGGGGTCGAGGCTTC

hTMEM165 Ex1as: GGTTCTTTGTTCCGGTGGCTAAG

hGb3S-Ex3s: ACCAGCCGGTTCCTGCTGGAAG

hGb3S-Ex3as: GGTTATAGAGCTGCCCTTTCTCC

Primers for constructing expression vectors (Underlines are indicative of restriction enzyme cutting sites)

hTM9SF2 BglII-ATGs: ACCAGATCTCCCGGGTATCATGAGCGCGAGGCTGC

hTM9SF2-XhoI-STOPas: ACCCTCGAGTCAGTCAACCTTCACCACACTG

hTM9SF2 XhoI-ENDas: ACCCTCGAGGTCAACCTTCACCACACTGTATATTTTG

hTM9SF1-SacI-ATGs: ACCGAGCTCAGGATGACAGTCGTAGGGAAC

hTM9SF1-XhoI-STOPas: ACCCTCGAGAACTCAGTCCATCTTGAGGTTAACATAG

hTM9SF3-SacI-ATGs: ACCGAGCTCAGGATGAGGCCGCTGCCT

hTM9SF3-XhoI-STOPas: ACCCTCGAGGGGTCTCTAGTCAATTTTCACATTAG

hTM9SF4-RI-ATGs: ACCGAATTCAAGATGGCGACGGCGATGGATTG

hTM9SF4-Xho-STOPas: ACCCTCGAGTCAGTCTATCTTCACAGCAGCATAGATC

hTM9SF2 SVN STOPas: ACCCTCGAGTCAATTAACAGACACCACACTGTATATTTTGGTAAC

hTM9SF2 AVA STOPas: ACCCTCGAGTCAAGCAACAGCCACCACACTGTATATTTTGGTAAC

hTM9SF2 CΔ3 STOPas: ACCCTCGAGTCACACCACACTGTATATTTTGGTAAC

hLAPTM4A BamHI-ATGs: ACCGGATCCACGATGGTGTCCATGAGTTTCAAGC

hLAPTM4A XhoI-STOPas: ACCCTCGAGTCAGGCAGGTAAGTAAGGAGGTG

hLAPTM4A XhoI-ENDas: ACCCTCGAGGGCAGGTAAGTAAGGAGGTGGTGG

hLAPTM4A XhoI-NCY(ΔC)as: ACCCTCGAGATAGCAGTTCCAAACACAGTTAATTAGATAAGCC

hLAPTM4B BamHI-ATGs: ACCGGATCCGCGATGACGTCACGGACTCGGGTC

hLAPTM4B XhoI-ENDas: ACCCTCGAGGGCAGACACGTAAGGTGGC

hTMEM165 BamHI-ATGs: ACCGGATCCTGGTGCTGACTGCTCCCTAAG

hTMEM165 XhoI-STOPas: ACCCTCGAGTTAAAAACCAGAATCAGGGCTTATAAATAGTGC

Gb3S XhoI-ATGs: GCGCTCGAGATACCATGTCCAAGCCCCCCG

Gb3S HindIII-ENDas: GCGAAGCTTCAAGTACATTTTCATGGCCTCGTGCGTC

mNeonGreenVec5side-s: CTGGTTTAGTGAACCGTCAGATCC

mNeonGreenVec3side-as: CCTCTACAAATGTGGTATGGCTG

mNeonGreenCTs: GCTGCGGACTGG**ACC**AGGTCGAAGAAGACT (bold: mutation site)

mNeonGreenCTas: CTTCTTCGACCT**GGT**CCAGTCCGCAGCGGT (bold: mutation site)

hTM9SF2 N-HAas (spHA-TM9SF2): GTCCGGGACGTCATATGGGTACAGGCCGGGCAGGTAGAAAGC (underlined: HA-tag sequence)

hTM9SF2 N-HAs (spHA-TM9SF2): TATGACGTCCCGGACTACGCGCCCGTCAACTTCTGCGA (underlined: HA-tag sequence)

Primers for RT-PCR and real-time PCR

TM9SF1: hTM9SF1-SacI-ATGs and hTM9SF1-XhoI-STOPas described above

TM9SF3: hTM9SF3-SacI-ATGs and hTM9SF3-XhoI-STOPas described above

TM9SF4: hTM9SF4-RI-ATGs and hTM9SF4-Xho-STOPas described above

Gb3S s: GGCAACATCTTCTTCCTGGAGACTTC

Gb3S as: CGAACTTCCACATGAGTGCGATCC

GAPDH s: GAGTCAACGGATTTGGTCGT

GAPDH as: TTGATTTTGGAGGGATCTCG

sgRNA target sequences

Figure 1B and Figure S1A-C

SPTSSA: ACTGAACACCGTCCGCTCCC

A4GalT (Gb3S): CCCGCTGCCTTGGGGCGCCC

LAPTM4A (v3): CCAGGATGATCGTCCCGGTG

ACACA: GAAGACCTTAAAGCCAATGC

COG4: TCTAGGGATTGCCCGCATTG

TM9SF2 (v2): TGTGAACAGACTTGATTCAG

VPS54: TACTTGCTCCAGATCTGTCC

CAMLG: ACAGCGCATCAACCGGATCA

GOSR1: TCAATACCTACTTTCGAAGG

UNC50: AATCTATGAGTACAACCCAA

GET4: ACGAGGCGCACCAGATGTAC

PI4KB: GTATGAGCCAGCTGTTCCGAA

TMEM165: GCAGCCGGGGCGCCGATGCG

NBAS: ATCATCACGAAAGCAATTCG

ZDHHC17: ATGGAATGACGCCTTTAATG

PTAR1: TAACCGGAGTCCCATAGTCC

AAED1: AATGTCACCCTTATAGTGAT

TRAPPC12: GCCCGCTCTTGCCGTAGCCC

ARL1: ATCAGAGTTAGTTGCCATGT

FURIN: TCACTCCTCGATGCCAGAAG

STX16: TTAGATCCAGAAGCAGCGAT

Figure 2A

TM9SF2 (v3): AAACAACTATCATGAGCGCG

LAPTM4A (v4): GCGGTTCCGCTTGAAACTCA

Figure S2E

A4GalT (C): CCATGAAAATGTACTTGTGA

Oligonucleotide for homologous recombination:

CTGGCCCAGCTGCATGCCCGCTACTGCCCCACGACGCACGAGGCCATGAAAATGTACTTGTACCCA

TACGATGTTCCAGATTACGCT**TGA**GGGGCCCGCCAGGTCACCTCCCCAACCTGCTCCTGATGGGGC

ACTGGGCCGCCCTTC (underline: HA-tag, bold: STOP codon)

Figure S5

TM9SF1: ATACAGAATAACAGGGTCGC

TM9SF3: CGTGCTCGTCCGCCCGGGTC

TM9SF4: TGATTTCTACGGGATCGTTC

Plasmids constructed in this study

$pCXN_2$-hTM9SF2 and spHA-TM9SF2 (and its mutants): cDNA (Blunt end-XhoI), plasmid (EcoRV-XhoI)

$pCXN_2$-hTM9SF2-HA: cDNA (Blunt end-XhoI), HA-tag (XhoI-NotI), plasmid (EcoRV-NotI),

$pCXN_2$-hTM9SF1 and hTM9SF3: cDNA (SacI-XhoI), plasmid (SacI-XhoI)

$pCXN_2$-hTM9SF4: cDNA (EcoRI-XhoI), plasmid (EcoRI-XhoI)

pMXs-IB-hLAPTM4A and hTMEM165: cDNA (BamHII-XhoI), plasmid (BamHI-XhoI)

pMXs-IB-hLAPTM4A-HA (and its mutant-HAs) and LAPTM4B-HA: cDNA (BamHII-XhoI),
HA-tag (XhoI-NotI), plasmid (BamHII-NotI)

pMXs-IB-HA-hLAPTM4A: HA-tag (BglII-BamHI), cDNA (BamHI-XhoI), plasmid (BamHI-XhoI)

pMXs-IP-Gb3S-moxNeonGreen (NG): Gb3S (XhoI-HindIII), NG (HindIII-NotI), plasmid (XhoI-NotI)

pMXs-IB-Gb3S-moxNeonGreen (NG): Gb3S (XhoI-HindIII), NG (HindIII-NotI), plasmid (XhoI-NotI)

pMXs-IP-B4G5-moxNeonGreen (NG): B4G5 (EcoRI-HindIII), NG (HindIII-NotI), plasmid (XhoI-NotI)

pMXs-IP-GM2S-moxNeonGreen (NG): GM2S (XhoI-HindIII), NG (HindIII-NotI), plasmid (XhoI-NotI)

pMXs-IP-B4G1-moxNeonGreen (NG): B4G1 (XhoI-HindIII), NG (HindIII-NotI), plasmid (XhoI-NotI)

pMXs-IP-MGAT1-moxNeonGreen (NG): MGAT1 (XhoI-HindIII), NG (HindIII-NotI), plasmid (XhoI-NotI)

pMXs-IP-Gb3S was constructed previously (Yamaji et al. 2010)

SUPPLEMENTAL REFERENCES

Bligh, E.G., and Dyer, W.J. (1959). A rapid method of total lipid extraction and purification. Can. J. Biochem. Physiol. 37, 911-917.

Caporaso, J.G., Kuczynski, J., Stombaugh, J., Bittinger, K., Bushman, F.D., Costello, E.K,, Fierer, N., Peña, A.G., Goodrich, J.K., Gordon, J.I., Huttley, G.A., Kelley, S.T., Knights, D., Koenig, J.E., Ley, R.E., Lozupone, C.A., McDonald, D., Muegge, B.D., Pirrung, M., Reeder, J., Sevinsky, J.R., Turnbaugh, P.J., Walters, W.A., Widmann, J., Yatsunenko, T., Zaneveld, J., and Knight, R. (2010). QIIME allows analysis of high-throughput community sequencing data. Nat. Methods 7, 335-336.

Jiang, H., Lei, R., Ding, S.W., and Zhu, S. (2014). Skewer: a fast and accurate adapter trimmer for next-generation sequencing paired-end reads. BMC Bioinformatics 15, 182.

Kawano, M., Kumagai, K., Nishijima, M., and Hanada, K. (2006). Efficient trafficking of ceramide from the endoplasmic reticulum to the Golgi apparatus requires a VAMP-associated protein-interacting FFAT motif of CERT. J. Biol. Chem. 281, 30279-30288.

Li, W., Xu, H., Xiao, T., Cong, L., Love, M.I., Zhang, F., Irizarry, R.A., Liu, J.S., Brown, M., and Liu, X.S. (2014). MAGeCK enables robust identification of essential genes from genome-scale CRISPR/Cas9 knockout screens. Genome Biol. 15, 554.

Morita, S., Kojima, T., and Kitamura, T. (2000). Plat-E: an efficient and stable system for transient packaging of retroviruses. Gene Ther. 7, 1063-1066.

Ogawa, M., Matsuda, R., Takada, N., Tomokiyo, M., Yamamoto, S., Shizukusihi, S., Yamaji, T., Yoshikawa, Y., Yoshida, M., Tanida, I., Koike, M., Murai, M., Morita, H., Takeyama, H., Ryo, A., Guan, J.L., Yamamoto, M., Inoue, J.I., Yanagawa, T., Fukuda, M., Kawabe, H., and Ohnishi, M. (2018). Molecular mechanisms of Streptococcus pneumoniae-targeted autophagy via pneumolysin, Golgi-resident Rab41, and Nedd4-1-mediated K63-linked ubiquitination. Cell Microbiol. , e12846.

Watanabe, M., Matsuoka, K., Kita, E., Igai, K., Higashi, N., Miyagawa, A., Watanabe, T., Yanoshita, R., Samejima, Y., Terunuma, D., Natori, Y., and Nishikawa, K. (2004). Oral therapeutic agents with highly clustered globotriose

for treatment of Shiga toxigenic Escherichia coli infections. J. Infect. Dis. 189, 360-368.

Yamaji, T., and Hanada, K. (2014). Establishment of HeLa cell mutants deficient in sphingolipid-related genes using TALENs. PLoS One 9, e88124.

Yamaji, T., Horie, A., Tachida, Y., Sakuma, C., Suzuki, Y., Kushi, Y., and Hanada, K. (2016). Role of Intracellular Lipid Logistics in the Preferential Usage of Very Long Chain-Ceramides in Glucosylceramide. Int. J. Mol. Sci. 17, E1761.